Solar Panel as a Receiver

A THESIS

SUBMITTED IN PARTIAL FULFILLMENT OF THE REQUIREMENTS FOR

THE DEGREE OF

M.Tech

BY

SANA ALI NAQVI

Electronics and Communication Engineering

Under the guidance of

Dr. Anand Srivastava (Advisor)
Dr. Abhijit Mitra (Co-Advisor)

July, 2020

Certificate

This is to certify that the thesis titled **"Solar Panel as a Receiver"** submitted by **Sana Ali Naqvi** for the partial fulfillment of the requirements for the degree of *Master of Technology* in *Electronics & Communication Engineering* is a record of the bonafide work carried out by her under my guidance and supervision in the Security and Privacy group at Indraprastha Institute of Information Technology, Delhi. This work has not been submitted anywhere else for the reward of any other degree.

Dr. Anand Srivastava(Advisor)
Department of ECE
IIIT-Delhi,
110020

Dr. Abhijit Mitra(Co-Advisor)
DST Inspire Faculty (ECE IIIT Delhi)
IIIT-Delhi,
110020

Acknowledgments

Towards the end of my M.Tech. degree, I would like to pay my gratitude to several individuals who contributed from various perspectives. First of all, I would like to express my profound gratitude to my thesis advisors, Dr. Anand Srivastava & Dr. Abhijit Mitra for their support, direction and motivation all along the way. They have been a great source of inspiration for me. Besides my advisors, I would like to thank the rest of my thesis committee: Dr. Vivek Bohara & Dr. Sayak Bhattacharya for their encouragement and insightful comments. I would like to express my gratitude towards my family for their kind co-operation and support which was a tremendous wellspring of motivation. Lastly, I need to thank my colleagues for all the mindful discourses we had, which incited me to think past the self-evident.

Abstract

In recent years solar panels are not only utilized for generating electricity and powering up the electrical devices, but also used as a medium to transfer information in a communication system. Solar panels, which are also photonic devices are getting popularity in various areas such as communication systems, power generations. While other photodetectors need an external power supply to operate, solar panel overcome this limitation by directly converting the optical to electrical signal. This work proposes the design of a receiver model using a solar panel as a photodetector. A reference circuit model is used for the analysis and results of the designed model are compared in terms of frequency response and Signal to Noise ratio. The analysis is done using theoretical calculations and by simulating the model in LTSpice. Signal to Noise ratio (SNR) due to the contribution of both thermal and shot noise also calculated for the reference as well as for the new designed model. To further improve the response at the output, an additional circuit of an equalizer is designed.

Contents

List of Figures

List of Tables

Chapter 1

Introduction

1.1 Motivation and objective

Optical Wireless Communication (OWC) is proving to be a promising technology which can be used as an alternative to Radio Frequency high-speed communication, which is already carved up.There are two essential parts in a communication system: transmitter and receiver. Visible Light Communication(VLC), which is a variant of Optical Wireless Communication, uses Light Emitting Diodes (LEDs) at the transmitter end for dual purpose of illumination and data transfer [2] [3]. Various photonic devices such as light-emitting diodes (LEDs), lasers, solar cells, and photodetectors can be used in power generation, optical communications, data transmission, etc. In a conventional OWC, photodiodes are used on the receiver end. The most common photodiodes used are positive-intrinsic-negative (PIN) photodiodes and avalanche photodiodes (APDs). However the main disadvantage of using them is the requirement of external power supply and convex lens to gather the light. To overcome this issue, photodiodes (PDs) can be replaced by solar panels.

Solar panels have a large receiving area, so they do not require convex lens,neither they need any external supply to operate. However, due to large area, the capacitance of the panel is also high which affects its response time [4]. Despite this disadvantage, several research studies proves that it is suitable as a receiver because it can be used for simultaneous energy harvesting and communication [5] [6] [1].

The DC component of the signal generated from the solar panel is used to power up the electronics devices or can be stored in a battery whereas the AC component of the signal is used for communication purposes. The work done in this literature includes:

1. Testing the solar panels to verify the pattern of the I-V characteristics and hence find the values of solar panel parameters (R_{sh} and R_s).

2. Implementation and verification of the circuit for both simultaneous energy harvesting and

communication [1] by simulating the same in LTSpice.

3. Designing a better receiver model for communication purpose with modifications in the existing circuit, using same solar panel which is used in the reference paper [1] and comparing the results to show how the designed model improves the performance of the system.

4. The factors that affect the Bandwidth and gain of the system are explained. The parameters that maximize performance are determined through simulations.

5. Calculated Signal to Noise ratio (SNR) of both reference and designed circuit due to the individual contribution of Shot and Thermal noise and by combining both (Shot and Thermal noise).

6. Initial phase of testing for improvising the shape of the output signal by adding an equalizer circuit is also performed.

1.2 Outline

The remaining thesis is organised as below:

Chapter 2 presents the analysis of the reference circuit with simultaneous energy harvesting and communication. The testing of solar panels and the results are shown.

Chapter 3 presents design of a new receiver model for communication purposes. Analysis of the factors that affects the system performance are discussed in detail. Improvements in the output response in terms of system bandwidth and shape of the output pulse is observed with the change in parameters.

Chapter 4 This chapter presents the noise analysis of the reference circuit and the designed circuit. The comparison is made on the grounds of Signal to Noise ratio. Preliminary stages of equalizer design for further improvement in output signal pulse shape is presented.

Chapter 5 This chapter concludes the thesis and suggests the possible directions for future work.

Chapter 2

Testing of solar panel and analysis of the factors affecting the system performance

2.1 Introduction

Solar cells, also known as photovoltaic cells (PV) converts the light energy directly into electricity by using photovoltaic effect. The solar cells are made of up semiconductor material such as silicon that absorb sunlight and convert it into electricity. When solar energy hits the cell, electrons from the material of solar cell knock out and create electron-hole pairs [7]. These carriers are separated by the internal electric field of the p-n junction and generates a current which is proportional to the radiation incident on the cells. In the absence of light, the I-V characteristic of a solar cell has an exponential characteristic similar to that of a diode [8]. Solar panels are made by combining these solar cells in a array of series and parallel combinations. There are variety of solar panels available according to their generations and material such as crystalline silicon, thin film solar cells etc.

Using an efficient solar panel is a must for getting a good response, which means the ability to receive an amount of solar energy and converting it into electricity. The efficiency of the cells depends on parameters such as irradiance and temperature [9]. The panel has maximum efficiency when it is fully illuminated. The equivalent model of a solar panel is shown in Figure 2.1. To analyse the performance of the panel, its unknown parameters need to be figured out first at Standard Test Conditions (STC) which are 25°C temperature and an irradiance of $1000 W/m^2$ [9]. The unknown parameters are:

- I_{ph}- the generated photocurrent

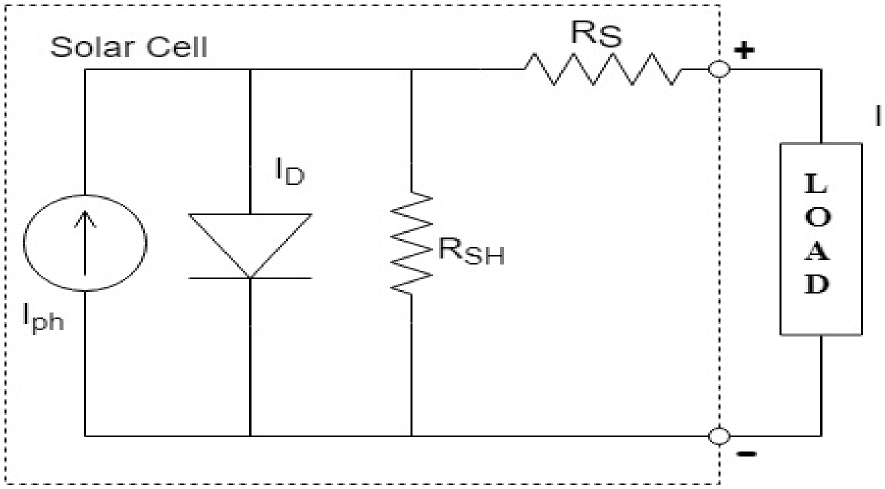

Figure 2.1: Equivalent model of a solar panel

- I_o- dark saturation current in STC
- R_s- panel series resistance
- R_{sh}- panel shunt resistance
- A- diode ideality factor

The shunt resistor R_{sh} accounts for the leakage around the edge of the cell, or at grain boundaries (interface between two crystallites, in a polycrystalline material), small metallic short circuits, diffusion paths along dislocations, etc. It represents any parallel high conductivity paths across the solar cell p–n junction. Practically it represents the leakage current. As can be seen from Figure 2.1, that for getting the maximum output current at the load, the current through this R_{sh} should be as low as possible. Therefore its value is kept high.
R_s represents the resistance due to metal contacts with the semiconductors, resistance of the layers of the semiconductors itself, loss due to cell interconnections, solder bonds, cell metallization, etc [10] [11]. If the value of R_s is kept high, the voltage drop across the load will decrease and so will be the current, therefore its value is kept low. These resistance values can be calculated using different techniques. One such method uses datasheet values provided along with the solar panel and solve equations at Short Circuit and Open Circuit conditions [9].Another technique is to plot the I-V characteristics of the solar panel and put that data in the following equation to extract the values [1] :-

$$I = I_{ph} - I_o(e^{\frac{V+IR_s}{n_s V_T}} - 1) - \frac{(V + IR_s)}{R_{sh}} \tag{2.1}$$

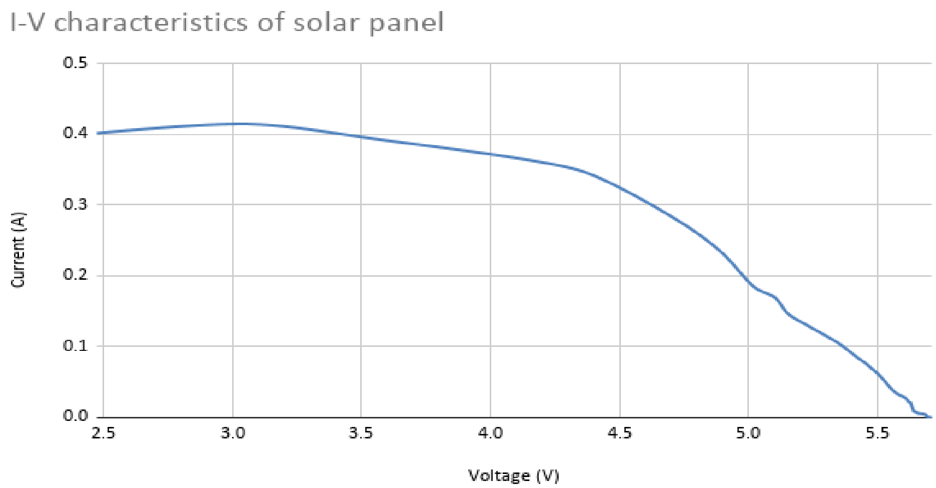

Figure 2.2: I-V graph of the tested solar panel

where V_T is junction thermal voltage of diode

$$V_T = \frac{AkT}{q} \tag{2.2}$$

The diode ideality factor is a measure of how closely the diode follows the ideal diode equation. During the study, few panels were also tested to analyse the pattern of I-V characteristics and hence find the parameters R_s and R_{sh}. The results are shown in Figure 2.2 for a 2.5W panel with open circuit voltage (V_{oc}) of 5.71V and short circuit current (I_{sc}) of 0.428A. The value of R_s and R_{sh} are obtained using MATLAB's GRABIT function. The slope is calculated at Short circuit and Open circuit point of this graph, with few approximations, explained below.

The I-V characteristic of the solar panel is given by equation (2.1), now for calculating the R_{sh} first, the dI/dV equation is derived from (2.1).

$$\frac{dI}{dV} = -\frac{I_o}{V_T}(e^{\frac{V+IR_s}{V_T}}(1 + R_s\frac{dI}{dV})) - \frac{1}{R_{sh}} - \frac{R_s}{R_{sh}}\frac{dI}{dV} \tag{2.3}$$

Keeping all dI/dV terms on the left side:

$$\frac{dI}{dV}(1 + \frac{R_s}{R_{sh}} + \frac{I_o R_s}{V_T}e^{\frac{V+IR_s}{V_T}}) = -\frac{I_o}{V_T}e^{\frac{V+IR_s}{V_T}} - \frac{1}{R_{sh}} \tag{2.4}$$

Now, considering only the following part of the above equation at Short Circuit condition:

$$I_o e^{\frac{V+IR_s}{V_T}} = I_o e^{\frac{I_{sc}R_s}{V_T}} \approx 0 \tag{2.5}$$

Here, V becomes 0 and I can be written as I_{sc}. Now assuming R_s to be too small, the exponential term becomes negligible. As I_o is of the order of nA, so the whole part is approximated as 0. Also as R_s is very low than R_{sh}, so the term (R_s/R_{sh}) is also considered as 0 in equation (2.4). Therefore, the slope is coming out to be:

$$\frac{dI}{dV} = -\frac{1}{R_{sh}} \tag{2.6}$$

Now for calculating R_s, the same equation (2.4) is considered here. Again taking the same term (2.5) at Open Circuit condition:

$$I_o e^{\frac{V+IR_s}{V_T}} = I_o e^{\frac{V_{oc}}{V_T}} = I_{sc} \tag{2.7}$$

Here, the I becomes 0, and V is replaced by V_{oc}. Now, this equation is actually the diode equation, and at open circuit, assuming that no external current will flow, so the entire short circuit current is the diode current, as the current through R_{sh} is also considered negligible which is given by V_{oc}/R_{sh} and as R_{sh} is considered as large, so this term is neglected. Now after applying this approximation, equation (2.7) becomes:

$$\frac{dI}{dV}(1 + R_s(\frac{1}{R_{sh}} + \frac{I_{sc}}{V_T})) = -(\frac{I_{sc}}{V_T} + \frac{1}{R_{sh}}) \tag{2.8}$$

One more approximation is taken, where assuming R_{sh} to be large enough, $1/R_{sh}$ term in the above equation is neglected too. And the final expression is coming out to be:

$$R_s = -\frac{dV}{dI} - \frac{V_T}{I_{sc}} \tag{2.9}$$

In MATLAB, figure 2.2 is used to find out the points at open circuit and short circuit, and the slope is calculated and put in the equations (2.6) and (2.9). The final values are coming out to be 197 ohm 3 ohm for R_{sh} and R_s respectively.

However, in the above testing, the value of R_{sh} is not that large as expected which is due to the damage in the solar panel during the experimentation.

2.2 Analysis of equivalent model for simultaneous energy harvesting and communication

The generated photocurrent from the solar panel consists of both AC and DC signal components, out of which DC is used for energy harvesting and AC for communication purpose. The reference paper presents the model with both energy harvesting and communication in an indoor

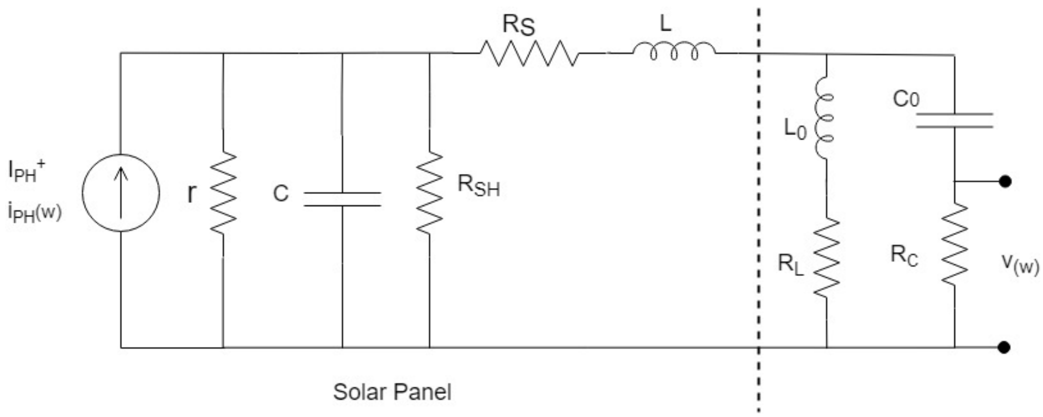

Figure 2.3: Circuit for both energy harvesting & communication [1]

environment. The circuit of the same is shown in Figure 2.3. In this section, the same model is implemented and compared with our design in the next section. The circuit is simulated in LT Spice simulation tool and the results are compared for different input frequencies. All the equations linked with this figure are solved in MATLAB.
The frequency response of the circuit can be evaluated using following equation [1]:

$$|\frac{v(w)}{i_{ph}(w)}|^2 = |\frac{\frac{R_X}{R_s+jwL+R_X}\frac{R_C}{\frac{1}{jwC_o}+R_C}}{\frac{1}{r}+jwC+\frac{1}{R_{sh}}+\frac{1}{R_s+jwL+R_X}}|^2 \tag{2.10}$$

where R_X is

$$R_X = \frac{1}{\frac{1}{jwL_o+R_L}+\frac{1}{\frac{1}{jwC_o}+R_C}} \tag{2.11}$$

2.3 Simulation of the model

The input signal generated at STC by the solar panel is 1.36 mA at 0.7x10$^{-3}W/cm^2$ irradiance level. The circuit is designed and simulated in LT Spice tool and the frequency response is shown in Figure 2.4. All the component values are mentioned in the circuit diagram of Figure 2.4 (a). The Bandwidth of this model was coming out to be around 1.53 MHz with a gain of -35.9 dB.

The frequency response of a system is dependent on the system parameters, i.e the component values used in the circuit. So with the change in the values of these parameters the results change. In the next chapter this analysis has been done with the new designed receiver model and compared with the response of this section.

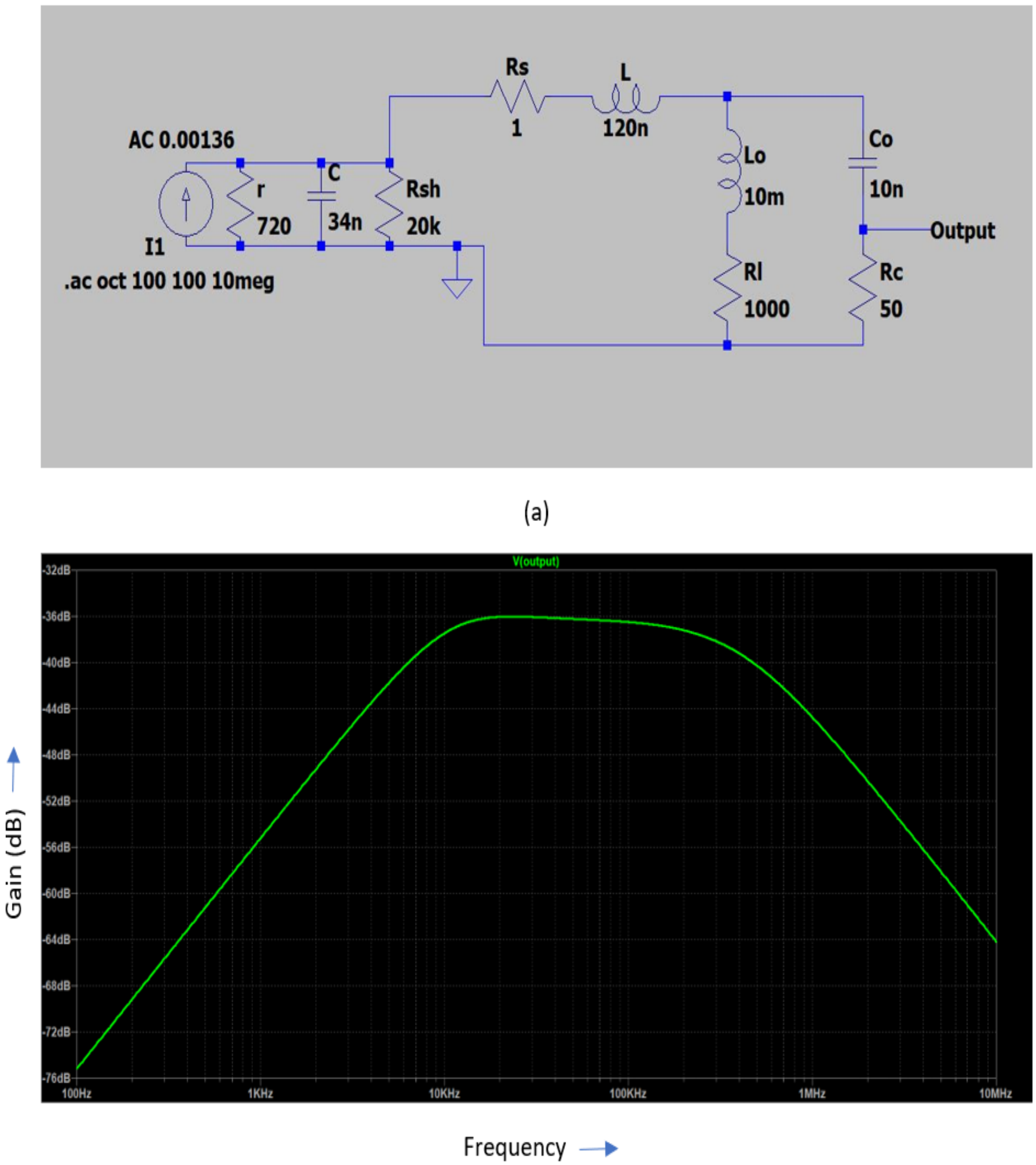

Figure 2.4: Model for simultaneous energy harvesting and communication [1]. (a) Circuit designed in LT Spice (b) Frequency response

Chapter 3

Simulation of Receiver circuit for communication

3.1 Introduction

This chapter focuses on designing the solar-panel based receiver model for communication purposes and analysing the factors which affect the response of the system. The energy harvesting part is not considered in this work. In this section, AC & Transient analysis of the reference circuit and the new designed receiver circuit is carried out. The performance of both the models is compared in the next section of this chapter. Same solar panel specifications are used throughout the study at the same irradiance level.

3.1.1 AC Analysis of the reference circuit

In this section, AC analysis of only the communication model of the reference paper is implemented and simulated in LT Spice [1]. The circuit of the receiver is shown in Figure 3.1. The elements in the circuit has following significance:

- r= small signal equivalent of the diode of solar panel
- C= to capture internal capacitive effects of solar cell
- L= inductance of wire connections with the panel
- R_c= load connected to the panel
- R_{sh}= shunt resistor of the panel
- R_s= series resistor of the panel

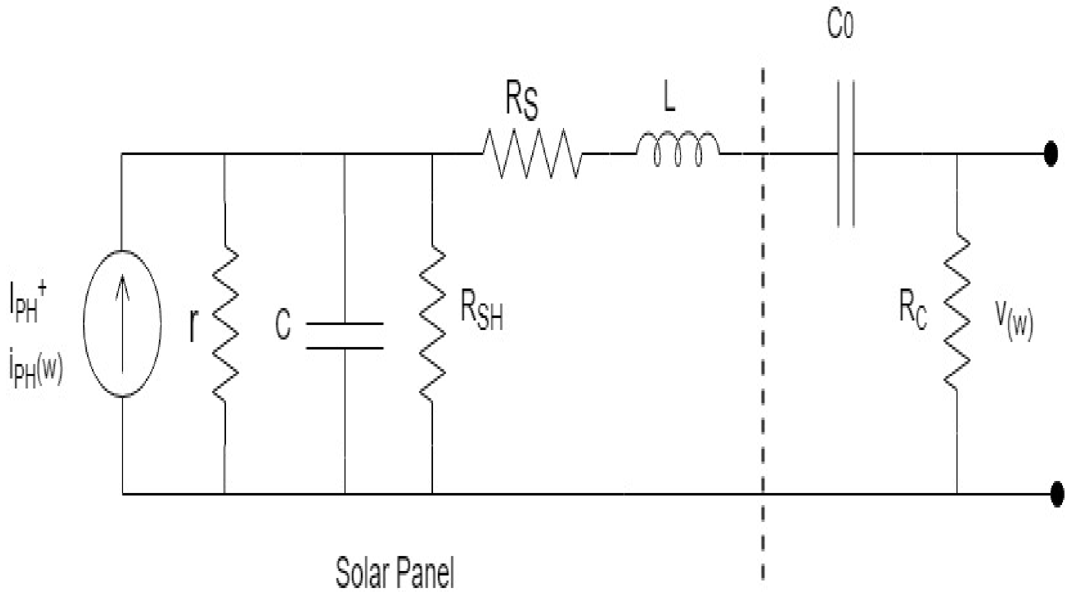

Figure 3.1: Communication model [1]

- C_o= capacitor to block the DC signal component

For analysing the communication model, only the AC component of signal is required, hence the DC signal is blocked by adding a capacitor C_o before the load. For observing the response of the model, following equation is derived and simulated in LT Spice. The input signal which is taken in this work is 1.36 mA and the received output signal is determined in terms of voltage across the load resistor R_c.

$$|\frac{v(w)}{i_{ph}(w)}|^2 = |\frac{\frac{R_c}{R_X}}{\frac{1}{r} + jwC + \frac{1}{R_{sh}} + \frac{1}{R_X}}|^2 \tag{3.1}$$

where

$$R_X = R_s + jwL + \frac{1}{jwC_o} + R_c \tag{3.2}$$

The frequency response of the system in Figure 3.2 show that the Bandwidth achieved with the given parameters is coming out to be 690 kHz with a 3-dB gain of -39.36 dB.

The same circuit is simulated for different values of load resistor (10/50/100/500 ohm) and capacitor (10nF/100nF/1uF) and the corresponding change in the gain and bandwidth of the system is shown in Figure 3.3 - 3.5.

- R_{sh}: 20kohm
- R_s: 1 ohm

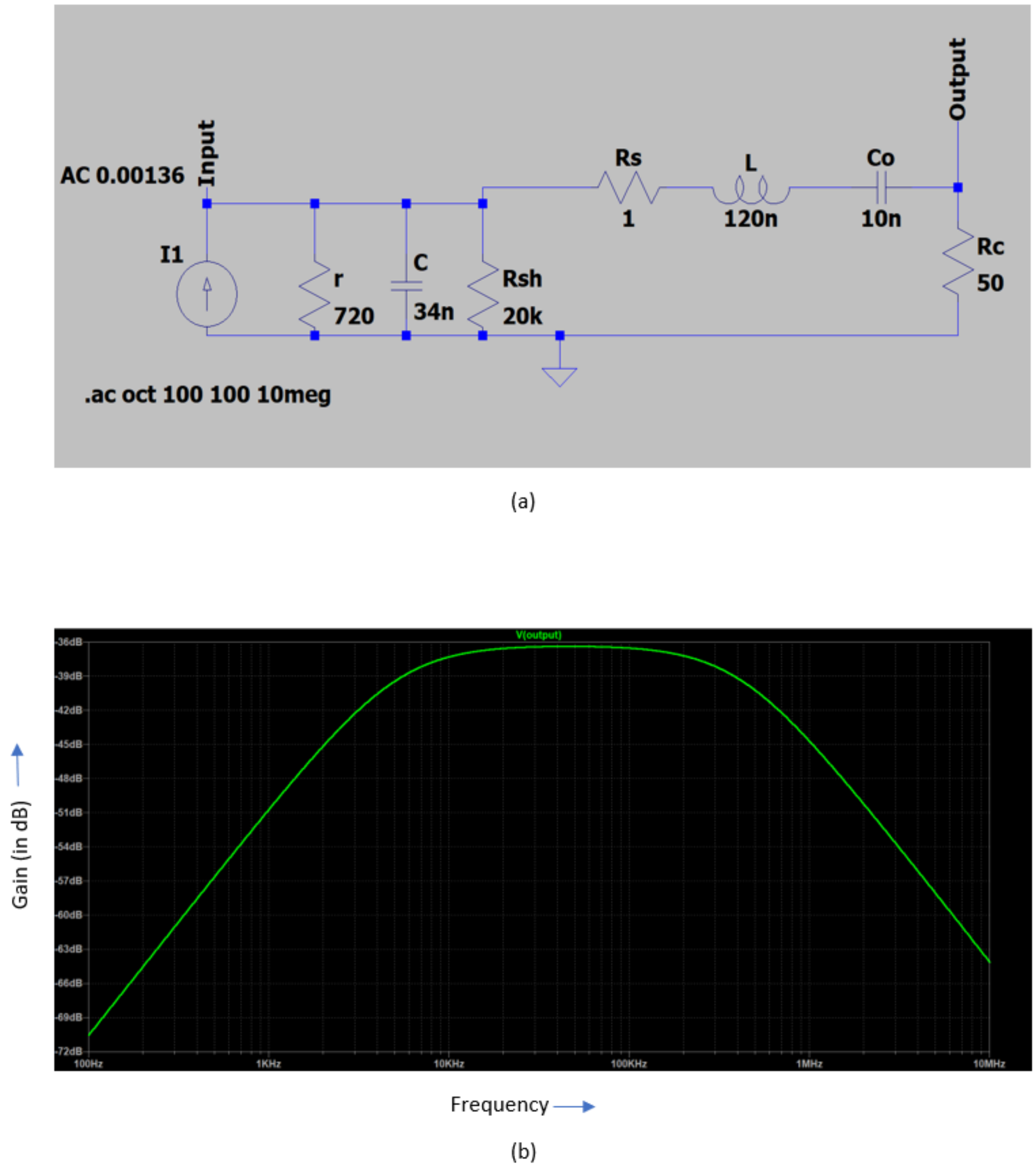

Figure 3.2: Communication model with $R_c = 50ohm$ and $C_o = 10nF$ [1] (a) Circuit designed in LT Spice (b) Frequency response

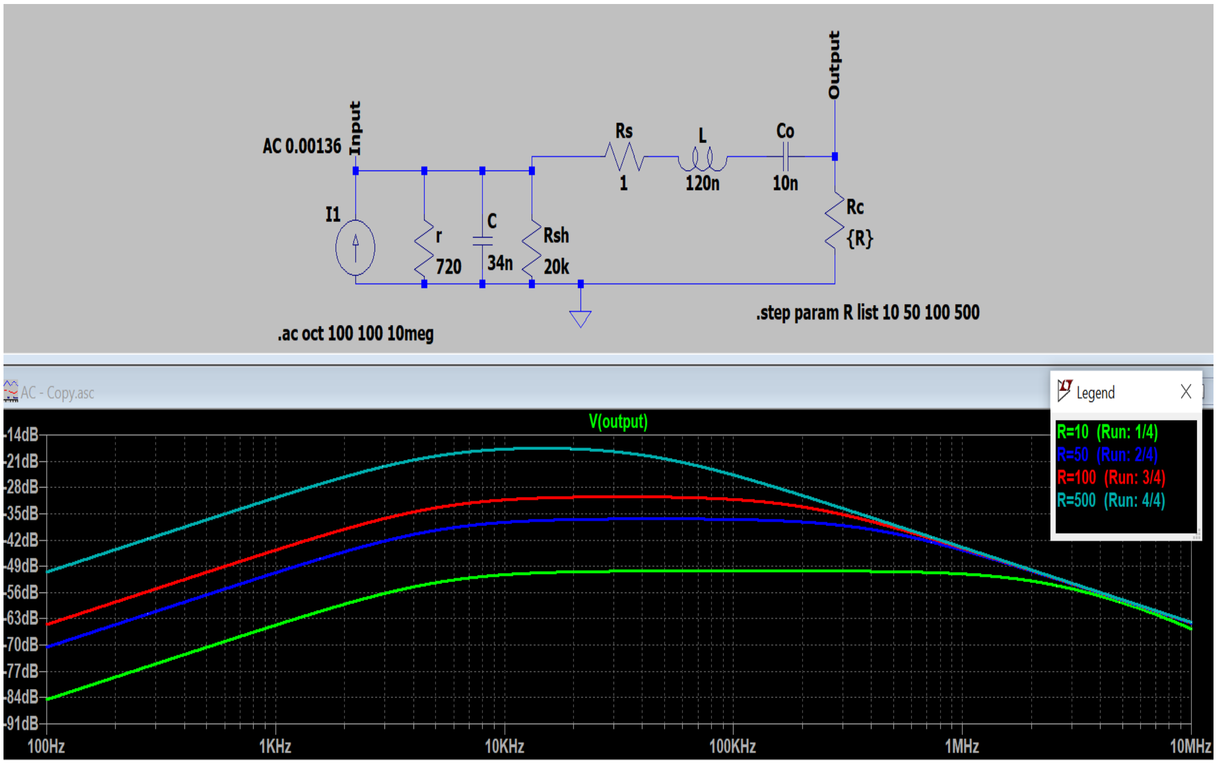

Figure 3.3: Communication model with $C_o = 10nF$ & $R_c = 10/50/100/500ohm$

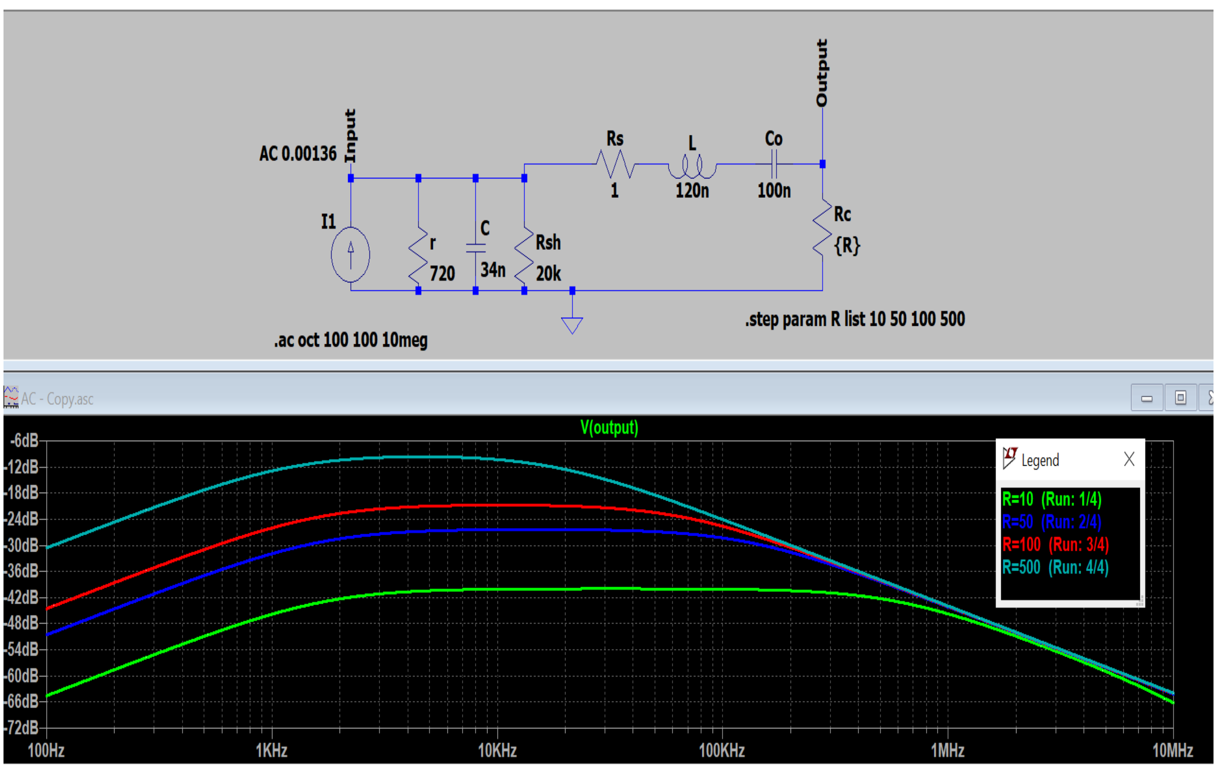

Figure 3.4: Communication model with $C_o = 100nF$ & $R_c = 10/50/100/500ohm$

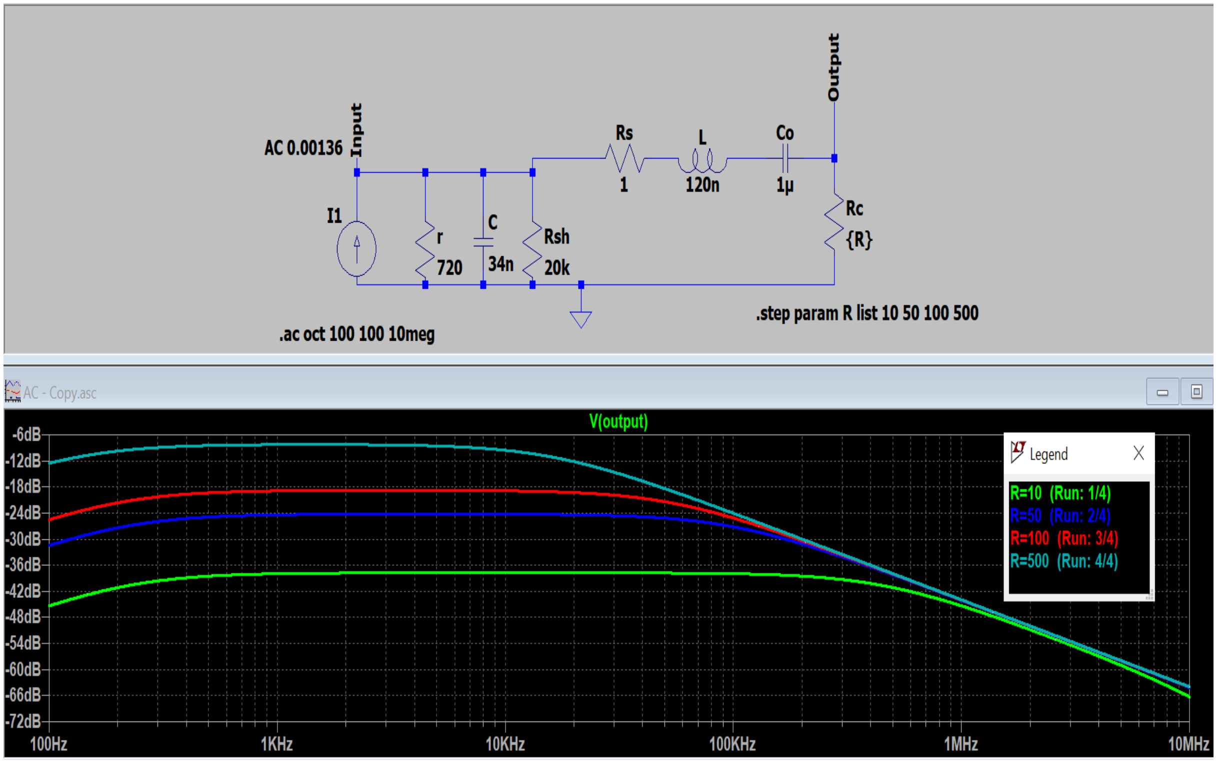

Figure 3.5: Communication model with $C_o = 1uF$ & $R_c = 10/50/100/500ohm$

- Irradiance : 0.7x$10^{-3}W/cm^2$
- r: 720 ohm
- C: 34nF
- L: 120nH
- R_c: 10/50/100/500 ohm
- C_o: 10nF/100nF/1uF

From these responses it can be concluded that with the increase in R_c the overall gain is increasing however the system Bandwidth is decreasing. Also, with the increase in C_o the response at low frequencies is improving. The final value taken for both R_c & C_o in this paper is 50ohm & 10nF respectively which is giving the best response out of all possible combinations [1].

3.1.2 Transient Analysis of the reference circuit

To measure the output received signal and to check the shape of pulse at different frequencies at the load resistor R_c, transient analysis of this circuit is performed. The square pulse is used as

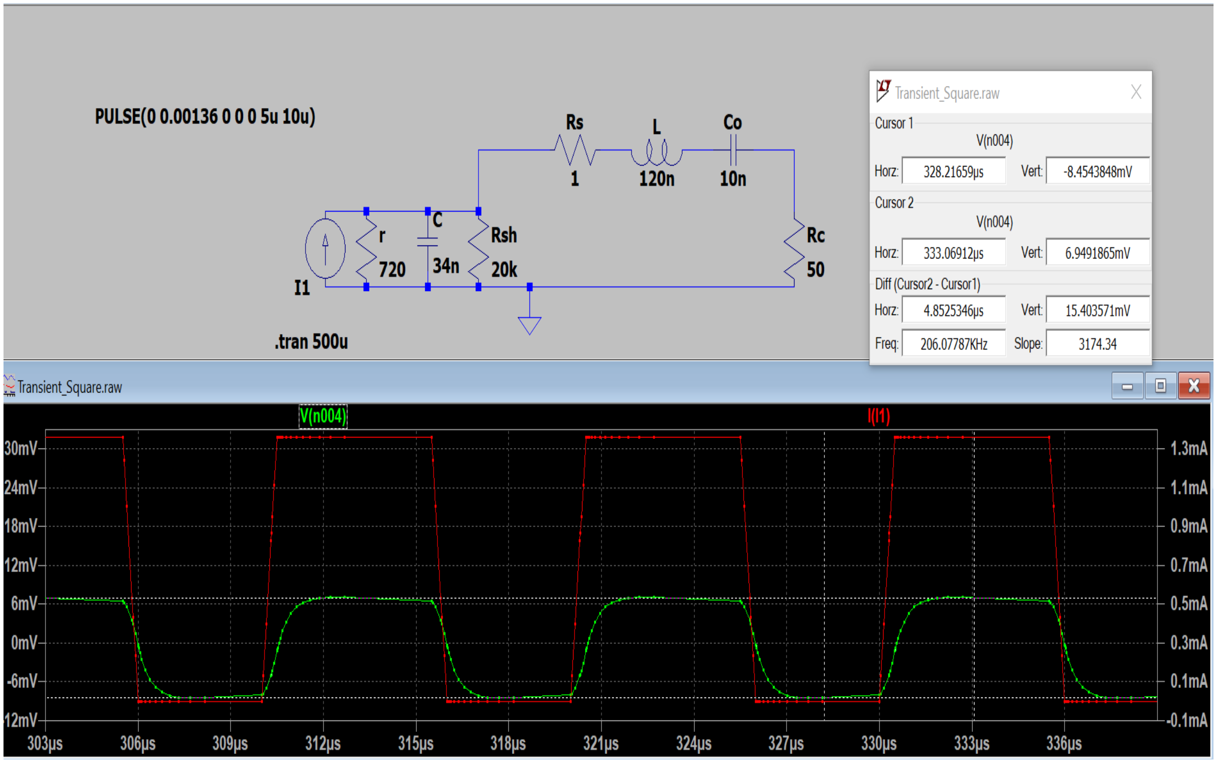

Figure 3.6: Transient analysis for 100kHz input frequency

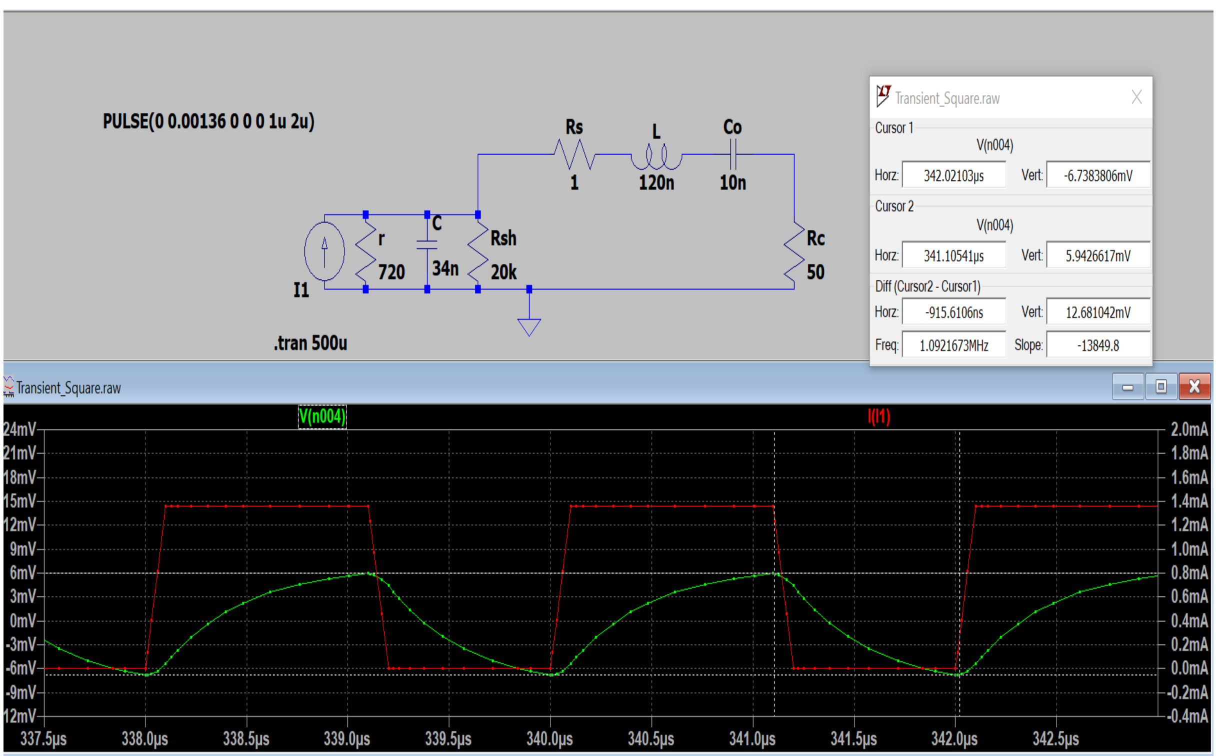

Figure 3.7: Transient analysis for 500kHz input frequency

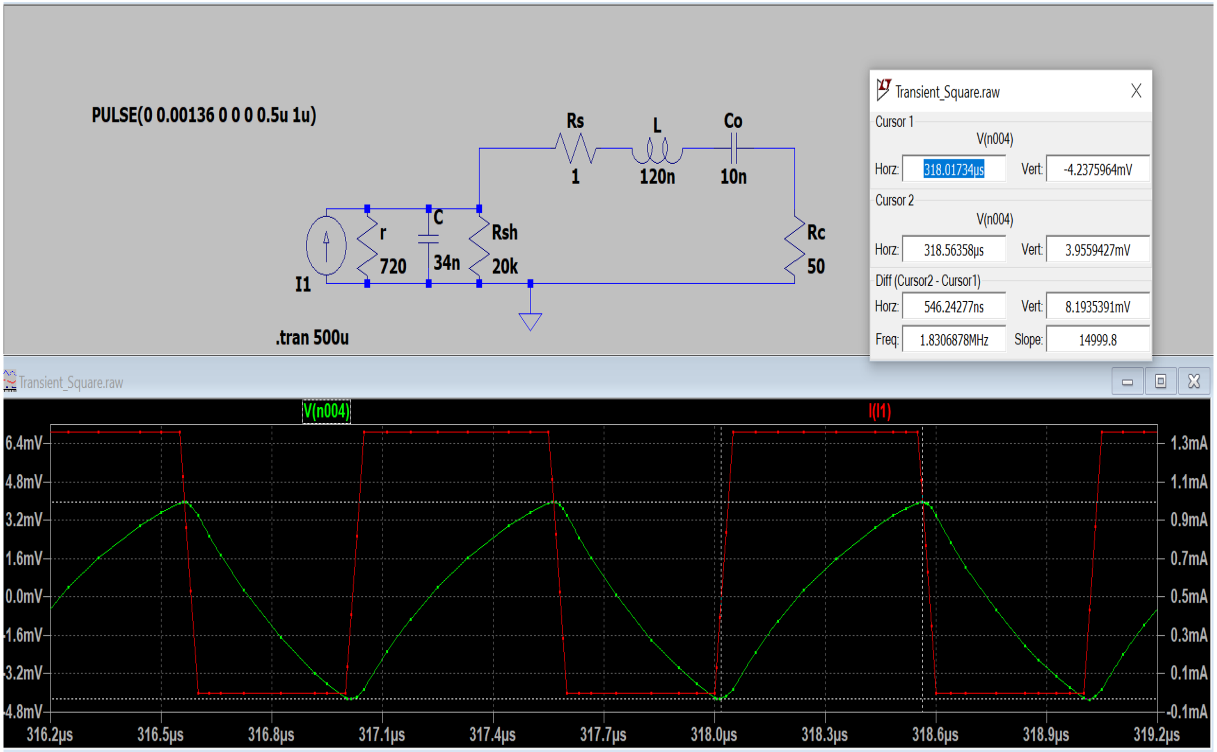

Figure 3.8: Transient analysis for 1MHz input frequency

the input signal. The results are shown in Figures 3.6 - 3.8 and the value of output voltages are shown in Table 3.1.

It can be seen from the results that with the increase in input frequency, the shape of the pulse deteriorate. Also, the value at the output signal is decreasing with the increase in frequency.

3.1.3 AC analysis of new circuit

As shown above that the system response is dependent on the load resistor and capacitor. The new receiver model designed for communication has modifications at this end, i.e the improved response is obtained when the value of load resistor and capacitor are set at 30 ohm and 5nF respectively. Equation for calculating the frequency response is given below. The result is shown in Figure 3.9, which gives a higher bandwidth of 2 MHz at a cost of decreased 3-dB gain of -48.6 dB.

$$|\frac{v(w)}{i_{ph}(w)}|^2 = |\frac{\frac{R_c}{R_X}}{\frac{1}{r} + jwC + \frac{1}{R_{sh}} + \frac{1}{R_X}}|^2 \tag{3.3}$$

where

$$R_X = R_s + jwL + \frac{1}{jwC_o} + R_c \tag{3.4}$$

Table 3.1: Output signal of reference model for different input frequencies

Frequency	Received signal at output load (R_c)
10 kHz	22.9 mV
100 kHz	15.4 mV
500 kHz	12.68 mV
1 MHz	8.19 mV
4 MHz	2.27 mV

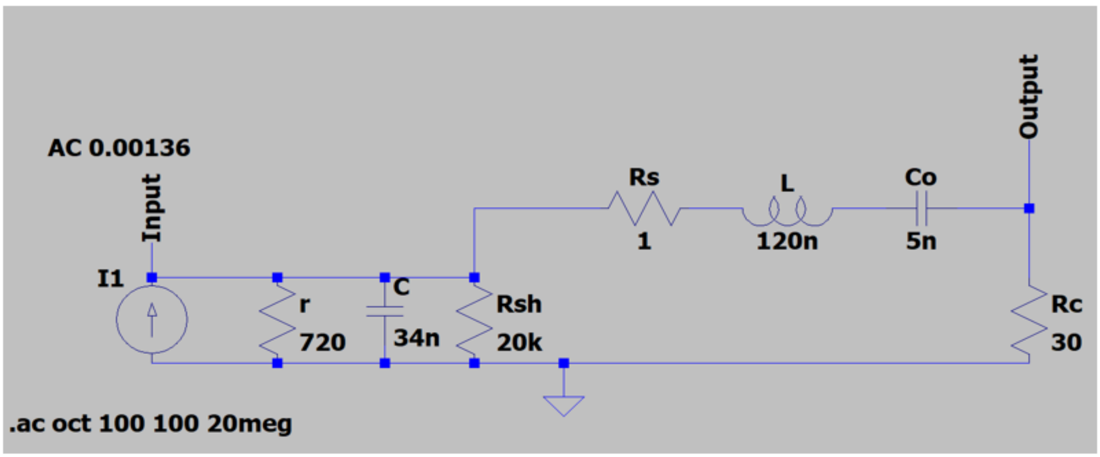

(a)

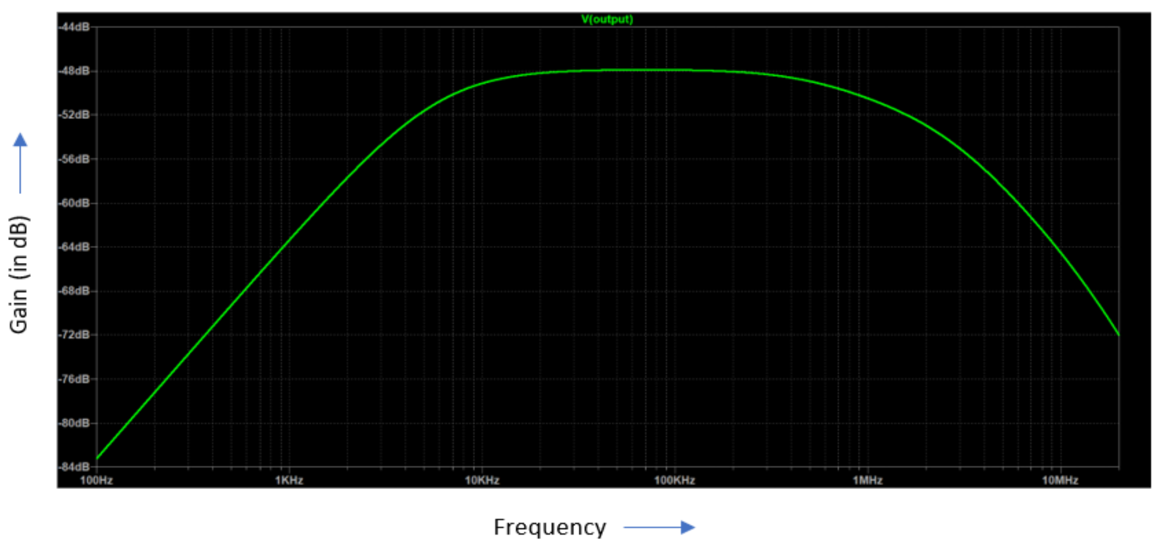

(b)

Figure 3.9: AC analysis of new designed circuit (a) Circuit Diagram (b) frequency response

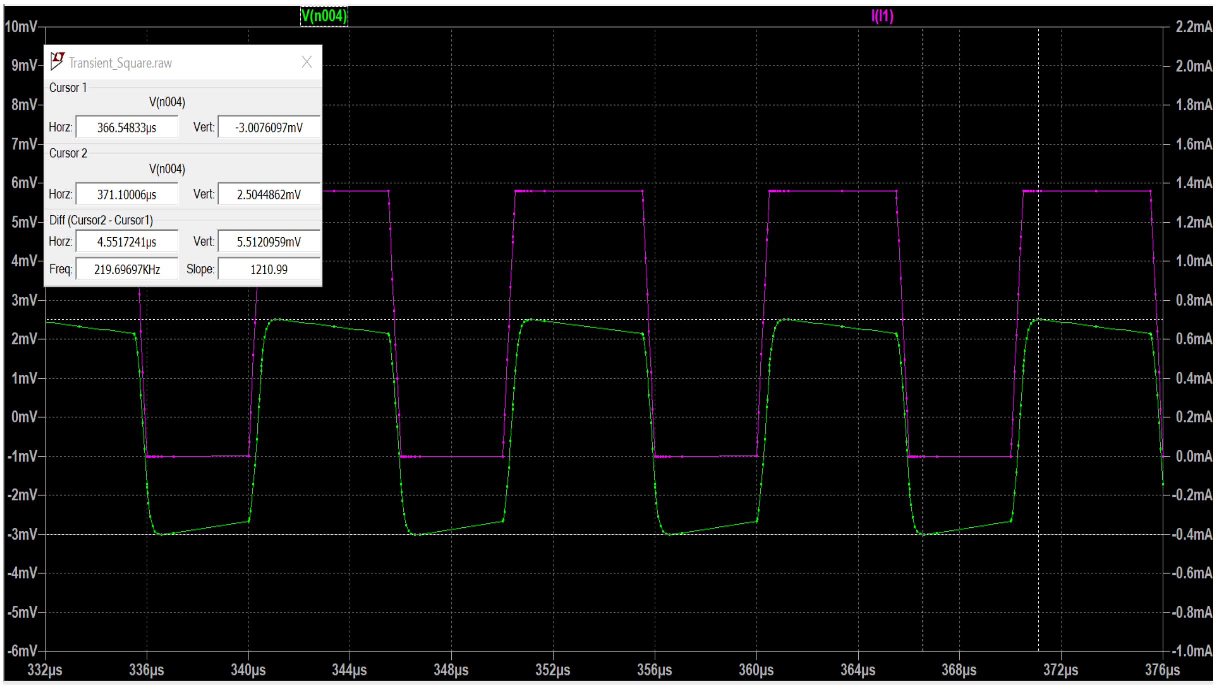

Figure 3.10: Transient analysis of new circuit for 100kHz input frequency

3.1.4 Transient analysis of new circuit

The transient analysis is done by giving the stream of square pulses (equal ON-OFF time) and observing the output signal at R_c. The results are shown in Figure 3.10 - 3.12 and the table of obtained output voltage at different input frequencies is shown in Table 3.2.

It can be seen from the results that however the output value is low as compared to the reference circuit but the shape of the output pulse is much better.

3.2 Random pulse at the input

The input pulse received by the panel may not always follow a same ON-OFF pattern, instead the data can be streamed in any random sequence. So this section will show the response when the pulse transmitted by the transmitter is random in nature. Figure 3.13 shows the output response for the bit stream (010000110011000101100) at 1MHz, 2MHz,3MHz & 4MHz. And it can be observed that even at random input data the output waveform is able to retain the shape.

3.3 Adding an Equalizer circuit to the model

An equalizer circuit attempts to recover the input signal which gets distorted during transmission through a channel. They are used to provide a flat frequency response from end to end. There

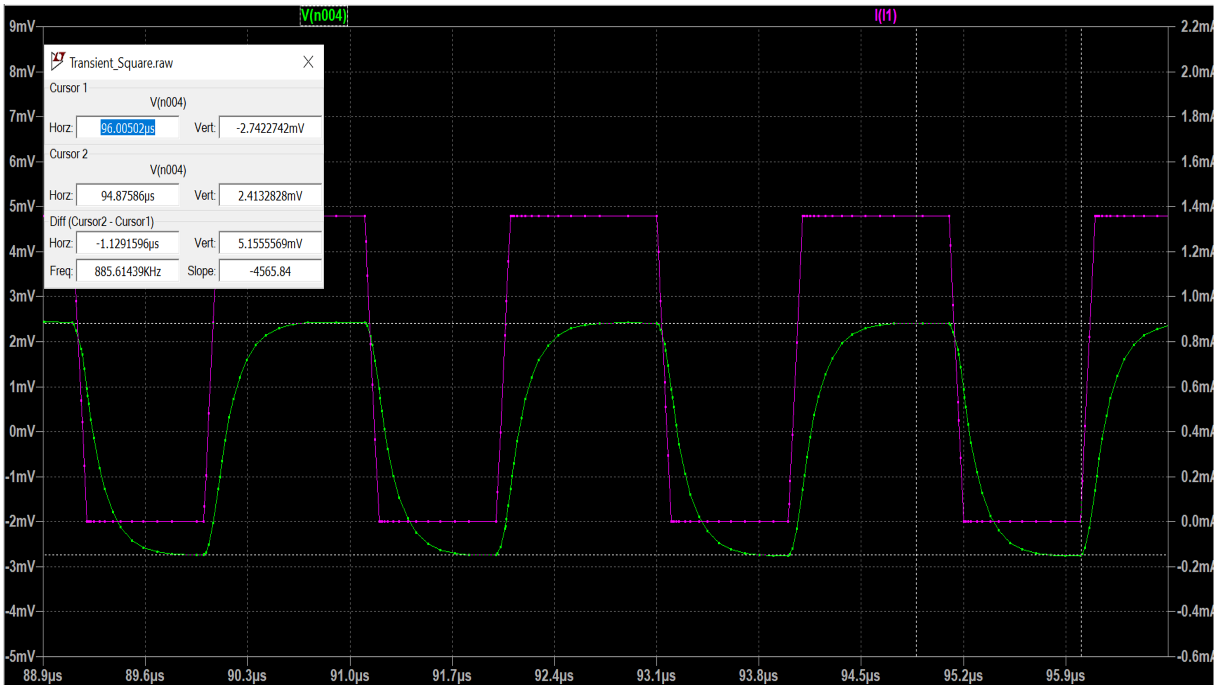

Figure 3.11: Transient analysis of new circuit for 500kHz input frequency

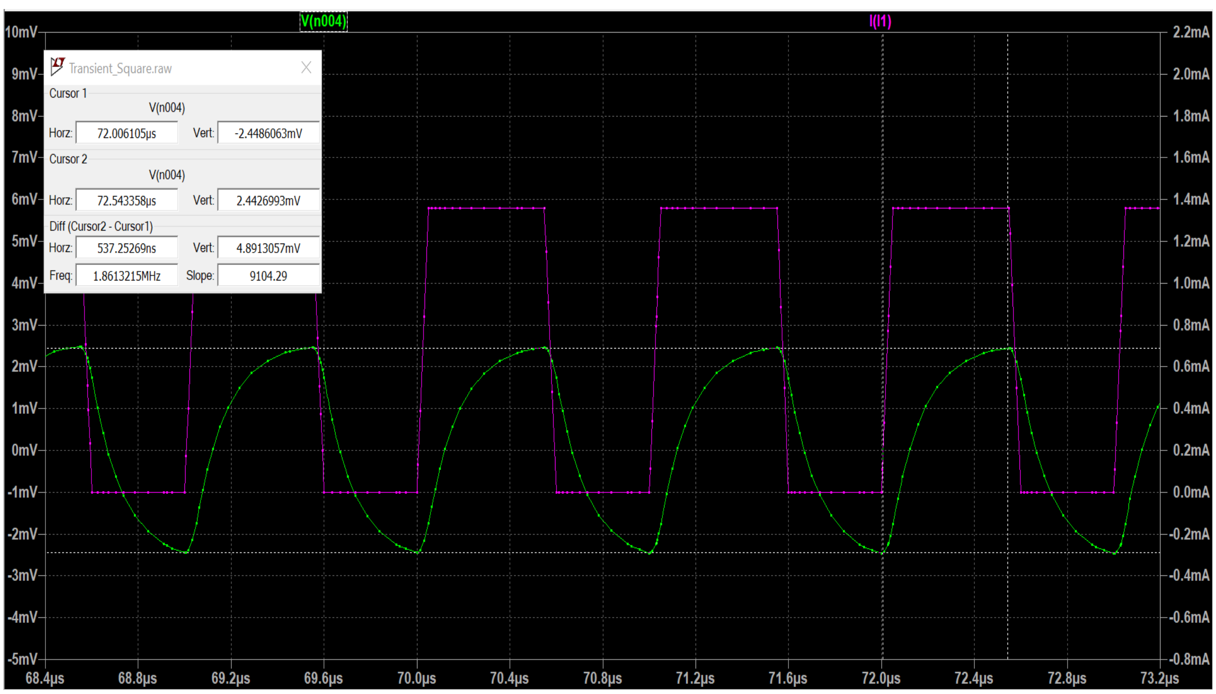

Figure 3.12: Transient analysis of new circuit for 1MHz input frequency

Table 3.2: Output signal of new model for different input frequencies

Frequency	Received signal at output load (R_c)
10 kHz	8.07 mV
100 kHz	5.51 mV
500 kHz	5.15 mV
1 MHz	4.89 mV
4 MHz	2.14 mV

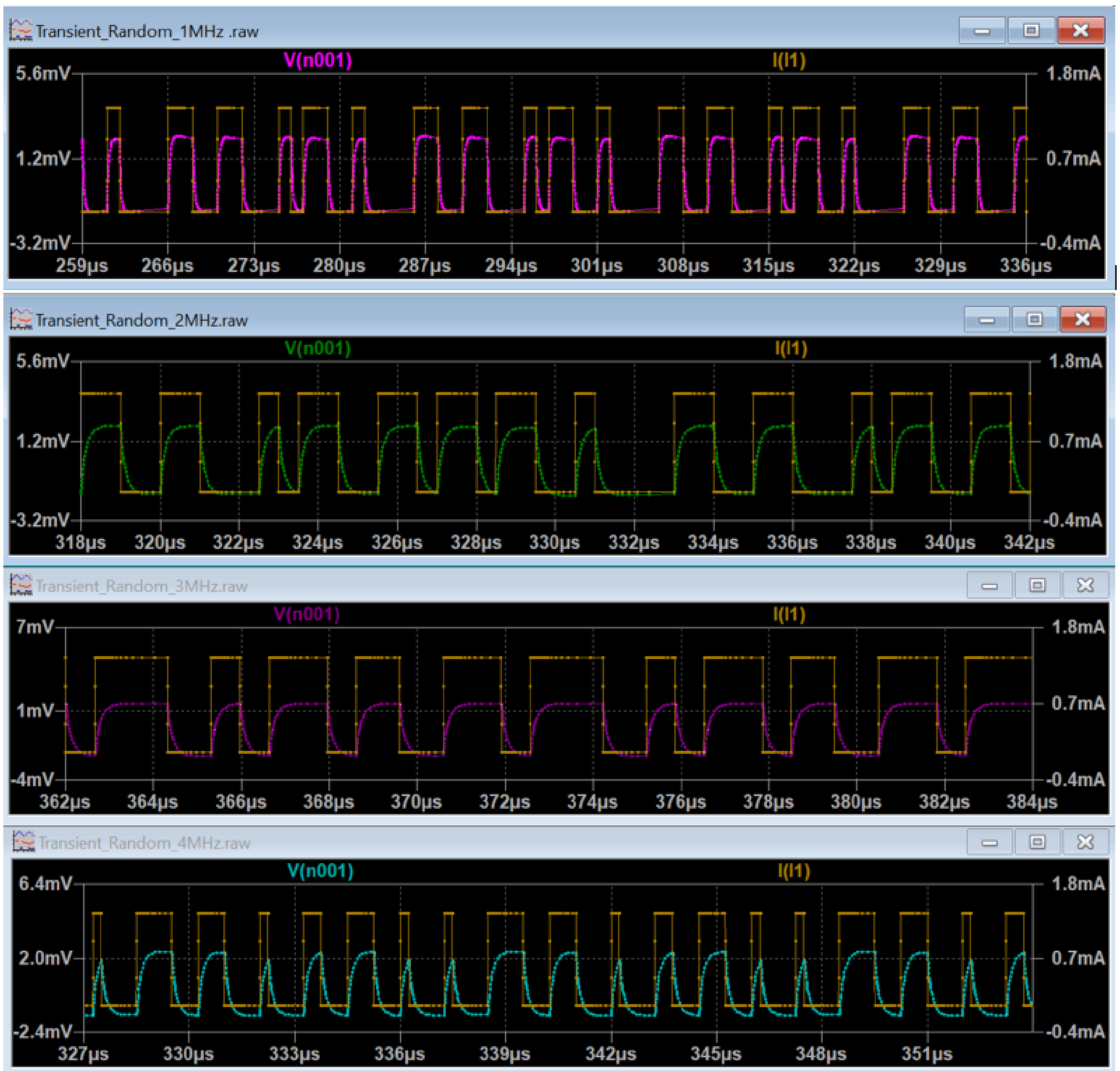

Figure 3.13: Random bit generated at the input at 1MHz, 2MHz, 3MHz & 4MHz from top to bottom

are variety of equalizers available for this purpose [12] [13]. The RC equalizer could be deployed as a pre-equalizer or post-equalizer.

An initial phase of testing is done by simulating the designed model after adding an RC post-equalizer circuit. Two equalizer circuits are designed and the responses are shown in Figure 3.14 and Figure 3.15 for 1 MHz.

With the decrease in equalizer capacitor (C1) and resistor (R1) values, the pulse shape is getting better. The output voltage however is lower than the value obtained before adding the equalizer. For Figure 3.14 it is coming out to be 2.54 mV and for Figure 3.15 it is 1.17 mV at 1 MHz input frequency. The comparison for different values of input frequency is shown in Figure 3.16. It can be seen from the chart that pulse shape is improved after adding the equalizer.

3.4 Results and Conclusion

This section will compare the AC and Transient analysis of reference model with the AC and Transient analysis of the new designed model. The comparison in terms of Gain, system Bandwidth, output voltage and shape of the output pulse is shown in Figure 3.17.

It can be concluded from the comparison chart that the Bandwidth achieved in this work is greater than the reference model. Also the shape of the output pulse is better in the new model.

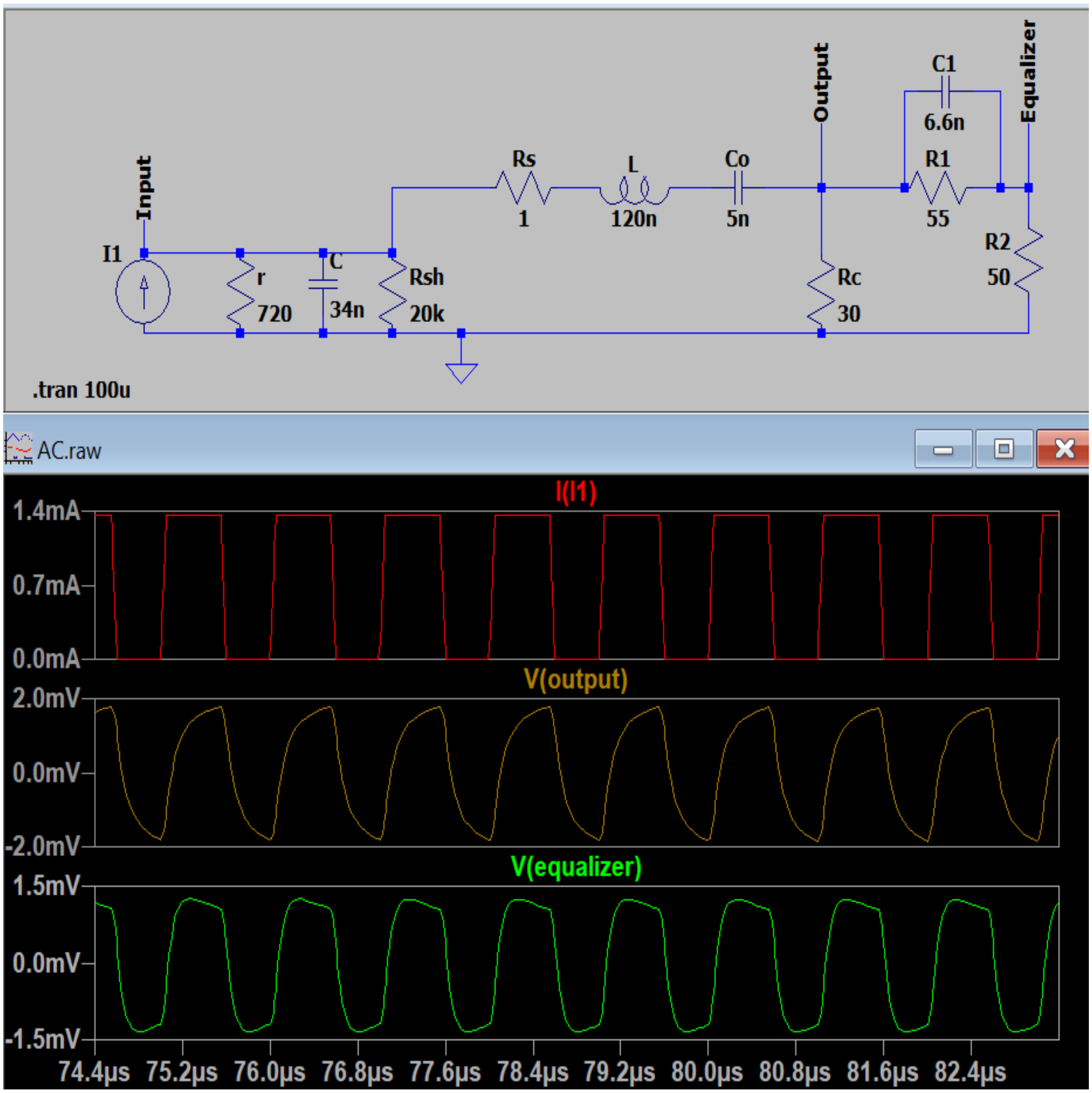

Figure 3.14: First circuit with the response before and after adding equalizer

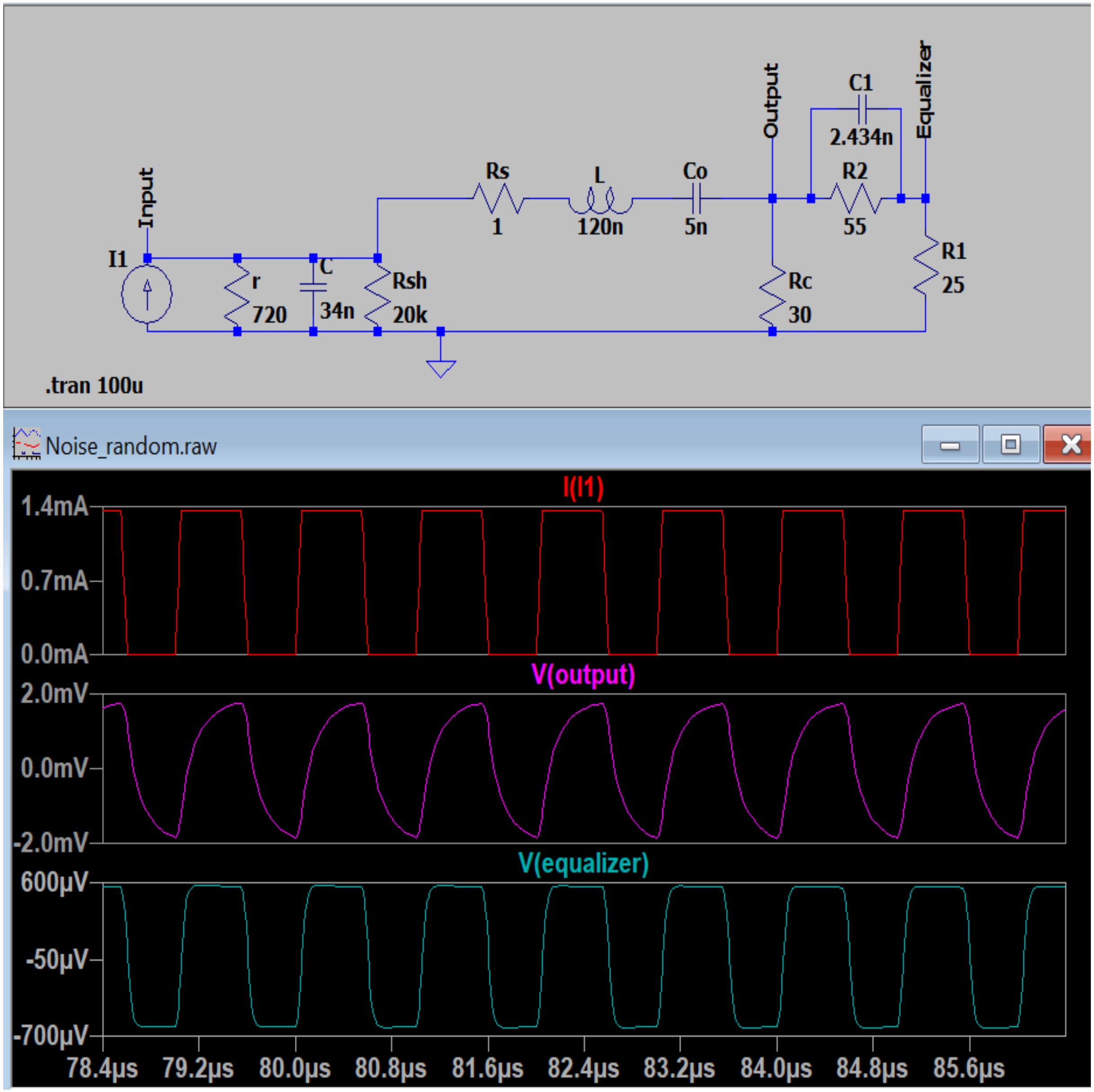

Figure 3.15: Second circuit with the response before and after adding equalizer

	Equalizer Circuit 1			Equalizer Circuit 2		
Output signal	500 kHz	1 MHz	2 MHz	500 kHz	1 MHz	2 MHz
Before	3.93 mV	3.51 mV	2.88 mV	3.73 mV	3.59 mV	2.79 mV
After	2.68 mV	2.54 mV	2.41 mV	1.18 mV	1.17 mV	1.14 mV
Output Waveform	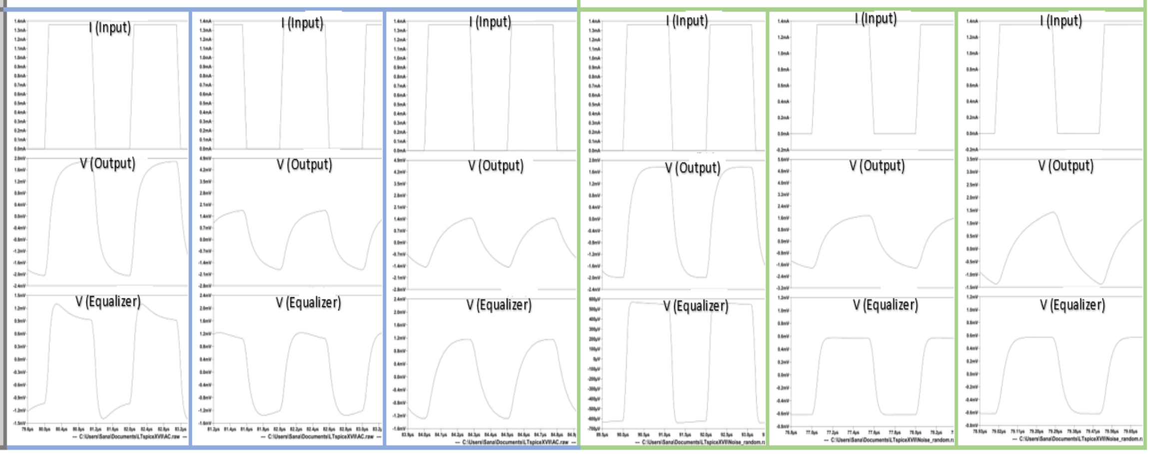					

Figure 3.16: Comparison between two equalizer designs

	Reference Circuit			This work		
Gain (in dB)	-39.36 dB			-48.6 dB		
Bandwidth	690 kHz			2 MHz		
Output signal	100 kHz	500 kHz	1 MHz	100 kHz	500 kHz	1 MHz
	15.4 mV	12.68 mV	8.19 mV	5.51 mV	5.15 mV	4.89 mV
Output Waveform	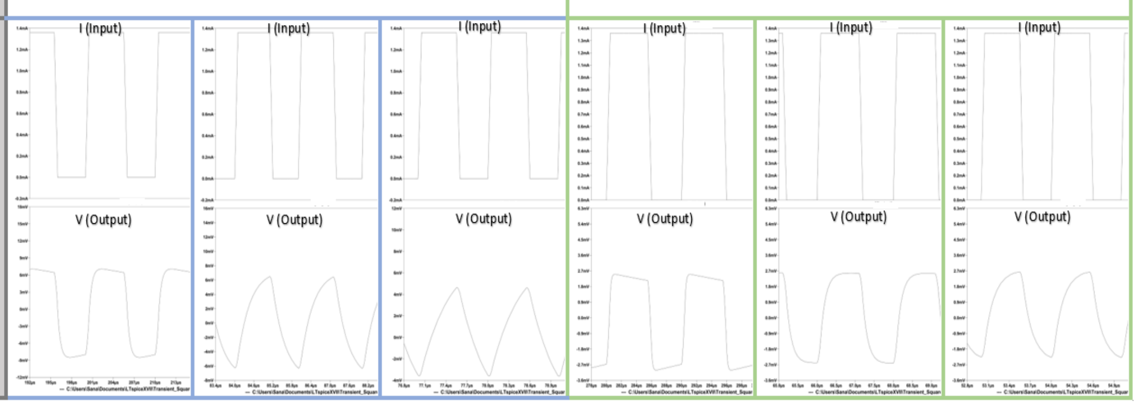					

Figure 3.17: Comparison chart of reference circuit and new circuit

Chapter 4

Noise Analysis

4.1 Introduction

Noise is an unwanted disturbance in the electrical signal. Different type of noises are generated by different type of sources. This section presents the Shot and Thermal noise analysis of the reference model and designed model and will compute the SNR due to both noises, individually and when both of them are taken into consideration together.

4.1.1 Shot Noise Analysis

Shot noise is caused due to flow of charge carriers. When the charge carriers try to cross a gap, the random fluctuations occur in the electric current, which causes a noise called Shot noise. If we talk about the circuit shown in Figure 2.3 and 3.1, the shot noise can be modelled as a current source in parallel with the current source of the solar panel [1]. Considered as a white noise, it has a flat Gaussian distribution and power spectral density (PSD) profile.

The PSD of the shot noise is given by following equation and the unit is A^2/Hz [14] [15]:

$$N_o^{shot} = 2q\rho\phi_a \tag{4.1}$$

where,

- q= charge of electron, 1.6x10^{-19} C
- ρ= responsivity of the solar panel, 4.5x10^{-3} A/W
- ϕ_a= light irradiance, 0.7x10^{-3} W/cm^2

In both the designs (reference model & designed model), solar panel with same specifications is used, so the parameters and the calculations will be same for both the models. With the known irradiance level and the area of the panel (432 cm^2) in this analysis, the solar power can be calculated from the following formula:

$$\phi_a = \frac{P_{in}}{Area^2} \tag{4.2}$$

Responsivity and the photocurrent are related by following equation:

$$I_p = \rho P_{in} \tag{4.3}$$

As the shot noise is a white noise, the variance of this noise can be calculated by multiplying it with the system Bandwidth.

Therefore, the variance of the shot noise is given by:

$$\sigma^2_{shot} = BN_o^{shot} \tag{4.4}$$

Using equations (4.1) & (4.4), the PSD and Variance of the shot noise are calculated as 1.009x$10^{-20}A^2/Hz$ and 5.04x$10^{-13}A^2$ respectively at a system Bandwidth of 50 MHz. The variance of the received information signal (1.36 mA) is 4.52x$10^{-8}A^2$.

So, the Signal to Noise ratio (SNR) for both the models due to Shot noise only can be calculated from:

$$SNR = \frac{SignalVariance}{NoiseVariance} \tag{4.5}$$

which is coming out to be 45.9 dB.

As it can be seen from equation (4.1) that the PSD is independent of input frequency, so for any input frequency it will be same, only the variance of the noise will change with respect to system Bandwidth, and so will be the SNR, which can be seen from Table 4.1.

4.1.2 Thermal Noise Analysis of Reference model

Thermal noise, also know as Johnson noise or Nyquist noise is generated inside an conductor due to the random thermal motion of charge carriers, which happens regardless of any applied voltage [15]. It is also considered as nearly a white noise because of the flat power spectral density upto 1 THz. Resistors are considered as main source of thermal noise.

In circuit 2.3, all five resistors will contribute to thermal noise. Thermal noise can be modelled as a voltage source in series with the resistor, whose noise is considered. The PSD due to

Table 4.1: SNR due to Shot noise only for both the models

Bandwidth	Variance of Shot noise	SNR in dB
100 kHz	1.009e-15	76.5
700 kHz	7.063e-15	68.1
1 MHz	1.009e-14	66.5
2 MHz	2.018e-14	63.5
4 MHz	4.036e-14	60.5
6 MHz	6.054e-14	58.7
10 MHz	1.009e-13	56.5
11 MHz	1.109e-13	56.1
15 MHz	1.51e-13	54.8
50 MHz	5.04e-13	49.5

contribution of all five resistors is calculated below:

1. **PSD due to resistor R_c**

$$N_{o,R_c}^{thermal} = 4kTR_c \tag{4.6}$$

where, T= 300K, Boltzmann constant k= 1.38x10^{-23} J/K, R_c= 50 ohm

Due to the presence of other electrical components in the circuit, this PSD needs to be multiplied with a factor which contributes in the enhancement of thermal noise due to these components.

$$|h_{R_c}(w)|^2 = |\frac{R_c}{R_c + \frac{1}{jwC_o} + \frac{1}{\frac{1}{R1} + \frac{1}{R_L + jwL_0}}}|^2 \tag{4.7}$$

where,

$R1 = \frac{1}{\frac{1}{\frac{1}{1/r + jwC + 1/R_{sh}} + R_s + jwL} + \frac{1}{R_L + jwL_o}}$

So, the total PSD due to R_c is given by

$$PSD_{Rc} = |h_{R_c}(w)|^2 N_{o,R_c}^{thermal} \tag{4.8}$$

2. **PSD due to resistor R_{sh}**

$$N_{o,R_{sh}}^{thermal} = 4kTR_{sh} \tag{4.9}$$

where, R_{sh}= 20 kohm

$$|h_{R_{sh}}(w)|^2 = |\frac{R3}{R_{sh}+R3} * \frac{R2}{R2+R_s+jwL} * \frac{R_c}{R_c+\frac{1}{jwC_o}}|^2 \tag{4.10}$$

where,

$R2 = \frac{1}{\frac{1}{R_c+\frac{1}{jwC_o}}+\frac{1}{R_L+jwL_o}}$, $R3 = \frac{1}{\frac{1}{jwL+R_s+R2}+\frac{1}{r}+jwC}$

So, the total PSD due to R_{sh} is given by

$$PSD_{Rsh} = |h_{R_{sh}}(w)|^2 N_{o,R_{sh}}^{thermal} \tag{4.11}$$

3. **PSD due to resistor r**

$$N_{o,r}^{thermal} = 4kTr \tag{4.12}$$

where, r= 720 ohm

$$|h_r(w)|^2 = |\frac{R5}{r+R5} * \frac{R4}{R4+R_s+jwL} * \frac{R_c}{R_c+\frac{1}{jwC_o}}|^2 \tag{4.13}$$

where,

$R4 = \frac{1}{\frac{1}{R_c+\frac{1}{jwC_o}}+\frac{1}{R_L+jwL_o}}$, $R5 = \frac{1}{\frac{1}{jwL+R_s+R4}+\frac{1}{R_{sh}}+jwC}$

So, the total PSD due to r is given by

$$PSD_r = |h_r(w)|^2 N_{o,r}^{thermal} \tag{4.14}$$

4. **PSD due to resistor R_s**

$$N_{o,R_s}^{thermal} = 4kTR_s \tag{4.15}$$

where, R_s= 1 ohm

$$|h_{R_s}(w)|^2 = |\frac{R6}{R_s + jwL + R7 + R6} * \frac{R_c}{R_c + \frac{1}{jwC_o}}|^2 \tag{4.16}$$

where,

$R6 = \frac{1}{\frac{1}{jwL_o + R_L} + \frac{1}{R_c + \frac{1}{jwC_o}}}$, $R7 = \frac{1}{\frac{1}{r} + jwC + \frac{1}{R_{sh}}}$

So, the total PSD due to R_s is given by

$$PSD_{R_s} = |h_{R_s}(w)|^2 N_{o,R_s}^{thermal} \tag{4.17}$$

5. **PSD due to resistor** R_L

$$N_{o,R_L}^{thermal} = 4kTR_L \tag{4.18}$$

where, R_L= 1000 ohm

$$|h_{R_L}(w)|^2 = |\frac{R_c}{R_c + \frac{1}{jwC_o}} * \frac{R8}{R_L + R8 + jwL_o}|^2 \tag{4.19}$$

where,

$R8 = \frac{1}{1/R10 + 1/R9}$, $R9 = R_c + \frac{1}{jwC_o}, R10 = \frac{1}{1/r + jwC + 1/R_{sh}} + R_s + jwL$

So, the total PSD due to R_L is given by

$$PSD_{R_L} = |h_{R_L}(w)|^2 N_{o,R_L}^{thermal} \tag{4.20}$$

Table 4.2: SNR due to Thermal noise only for the reference circuit

Input Frequency	Signal Variance at R_c	Thermal Noise Variance at B=50 MHz	SNR (in dB)	
			B=50 MHz	B=11 MHz
10kHz	4.4118e-06	2.1572e-13	73.1	79.6
20kHz	6.1240e-06	3.6994e-13	72.2	78.8
100kHz	5.5100e-06	3.8922e-12	61.5	68.1
300kHz	3.7638e-06	1.9413e-11	52.9	59.4
500kHz	2.3164e-06	2.9129e-11	49	55.6
700kHz	1.4692e-06	3.3944e-11	46.3	52.9
1MHz	8.2670e-07	3.7393e-11	43.4	50
2MHz	2.3128e-07	4.0722e-11	37.5	44.1
4MHz	5.9448e-08	4.1800e-11	31.5	38.1
6 MHz	2.6457e-08	4.2017e-11	27.9	34.5
10MHz	9.4204e-09	4.2122e-11	23.4	30
11MHz	7.7525e-09	4.2130e-11	22.6	29.2

Now, for calculating the total variance due to Thermal noise, all the PSDs due to individual resistors are added and multiplied with the system Bandwidth.

So, adding equation (4.8), (4.11), (4.14), (4.17) and (4.20), the total PSD obtained is:

$$N_o^{thermal} = PSD_{Rc} + PSD_{Rsh} + PSD_r + PSD_{Rs} + PSD_{RL} \tag{4.21}$$

and variance due to Thermal noise is calculated as:

$$\sigma^2_{thermal} = BN_o^{thermal} \tag{4.22}$$

The total received signal variance is calculated using the LRC gain from equation (2.3):

Total Signal Variance at output R_c= Input signal variance (4.52 x 10^{-8}) x LRC gain V^2.

As it can be seen from equations (2.3) and (4.21) that the LRC gain and thermal noise has a frequency factor, so Table 4.2 shows the variation in SNR due to Thermal noise only at different input frequencies and for different Bandwidths (B).

4.1.3 Thermal Noise Analysis of designed model

In this section, the Thermal noise analysis for the circuit given in Figure 3.1 is performed. Unlike the previous section, where the circuit involves energy harvesting branch also, this model has only four resistors (R_c, R_{sh}, r, R_s) and so the Thermal noise will occur due to these resistors only. The PSD due to contribution of these four resistors is calculated below:

1. **PSD due to resistor R_c**

$$N_{o,R_c}^{ther} = 4kTR_c \tag{4.23}$$

where, T= 300K, Boltzmann constant k= 1.38x10^{-23} J/K, R_c= 30 ohm

Due to the presence of other electrical components in the circuit, the factor which has to be multiplied with the above calculated PSD is given by:

$$|h_{R_c}(w)|^2 = |\frac{R_c}{R_c + \frac{1}{jwC_o} + Rn1}|^2 \tag{4.24}$$

where,

$Rn1 = R_s + jwL + \frac{1}{1/r+1/R_{sh}+jwC}$

So, the total PSD due to R_c is given by

$$PSD_{R_c}^{new} = |h_{R_c}(w)|^2 N_{o,R_c}^{ther} \tag{4.25}$$

2. **PSD due to resistor R_{sh}**

$$N_{o,R_{sh}}^{ther} = 4kTR_{sh} \tag{4.26}$$

where, R_{sh}= 20 kohm

$$|h_{R_{sh}}(w)|^2 = |\frac{Rn3}{R_{sh} + Rn3} * \frac{Rn2}{Rn2 + R_s + jwL} * \frac{R_c}{R_c + \frac{1}{jwC_o}}|^2 \tag{4.27}$$

where,

$Rn2 = R_c + \frac{1}{jwC_o}$, $Rn3 = \frac{1}{\frac{1}{jwL+R_s+Rn2}+\frac{1}{r}+jwC}$

So, the total PSD due to R_{sh} is given by

$$PSD_{R_{sh}}^{new} = |h_{R_{sh}}(w)|^2 N_{o,R_{sh}}^{ther} \tag{4.28}$$

3. **PSD due to resistor r**

$$N_{o,r}^{ther} = 4kTr \tag{4.29}$$

where, r= 720 ohm

$$|h_r(w)|^2 = |\frac{Rn5}{r + Rn5} * \frac{Rn4}{Rn4 + R_s + jwL} * \frac{R_c}{R_c + \frac{1}{jwC_o}}|^2 \tag{4.30}$$

where,

$Rn4 = R_c + \frac{1}{jwC_o}$, $Rn5 = \frac{1}{\frac{1}{jwL+R_s+Rn4}+\frac{1}{R_{sh}}+jwC}$

So, the total PSD due to r is given by

$$PSD_r^{new} = |h_r(w)|^2 N_{o,r}^{ther} \tag{4.31}$$

4. **PSD due to resistor R_s**

$$N_{o,R_s}^{ther} = 4kTR_s \tag{4.32}$$

where, R_s= 1 ohm

$$|h_{R_s}(w)|^2 = |\frac{Rn6}{R_s + jwL + Rn7 + Rn6} * \frac{R_c}{R_c + \frac{1}{jwC_o}}|^2 \tag{4.33}$$

where,

Table 4.3: SNR due to Thermal noise only for the designed model

Input Frequency	Signal Variance at R_c	Thermal Noise Variance at B=50 MHz	SNR (in dB)			
			B=50 MHz	B=11 MHz	4 MHz	2 MHz
10kHz	4.9650e-07	1.4956e-14	75.2	81.7	86.1	89.1
20kHz	6.1453e-07	2.3284-14	74.2	80.7	85.1	88.1
100kHz	6.6088e-07	1.8930e-13	65.4	72	76.3	79.4
300kHz	6.2902e-07	1.4830e-12	56.2	62.8	67.2	70.2
500kHz	5.7081e-07	3.7103e-12	51.8	58.4	62.8	65.8
700kHz	5.0111e-07	6.3709e-12	48.9	55.5	59.9	62.9
1MHz	3.9780e-07	1.0310e-11	45.8	52.4	56.8	59.8
2MHz	1.7956e-07	1.8600e-11	39.8	46.4	50.8	53.8
4MHz	5.5848e-08	2.3136e-11	33.8	40.4	44.7	47.8
6 MHz	2.5724e-08	2.3977e-11	30.3	36.8	41.2	44.2
10MHz	9.1414e-09	2.3667e-11	25.8	32.4	36.8	39.8
11MHz	7.4812e-09	2.3436e-11	25	31.6	36	39

$Rn6 = R_c + \frac{1}{jwC_o}$, $Rn7 = \frac{1}{\frac{1}{r}+jwC+\frac{1}{R_{sh}}}$

So, the total PSD due to R_s is given by

$$PSD_{R_s}^{new} = |h_{R_s}(w)|^2 N_{o,R_s}^{ther} \tag{4.34}$$

Adding equation (4.25), (4.28), (4.31) and (4.34), the total PSD obtained is:

$$N_o^{ther} = PSD_{R_c}^{new} + PSD_{R_{sh}}^{new} + PSD_{r}^{new} + PSD_{R_s}^{new} \tag{4.35}$$

and variance due to Thermal noise is calculated as:

$$\sigma_{ther}^2 = BN_o^{ther} \tag{4.36}$$

The total received signal variance is calculated using the LRC gain from equation (3.1):

Total Signal Variance at output R_c= Input signal variance (4.52 x 10^{-8}) x LRC gain V^2.

Table 4.3 shows the variation in SNR due to Thermal noise only, at different input frequencies and for different Bandwidths (B).

Table 4.4: SNR due to Shot+Thermal noise for 50 MHz bandwidth (reference model)

Frequency	Signal Variance (A^2)	Shot noise Variance (A^2)	Thermal Noise (V^2)	Gain (R^2)	Thermal Noise Variance (A^2)	SNR in dB
10 kHz	4.52e-8	5.04e-13	2.15e-13	97.6	2.2e-15	49.5
100 kHz	4.52e-8	5.04e-13	3.89e-12	121.9	3.19e-14	49.3
700 kHz	4.52e-8	5.04e-13	3.39e-11	32.5	1.04e-12	44.7
1 MHz	4.52e-8	5.04e-13	3.73e-11	18.2	2.04e-12	42.5
2 MHz	4.52e-8	5.04e-13	4.07e-11	5.1	7.98e-12	37.3
4 MHz	4.52e-8	5.04e-13	4.18e-11	1.3	3.21e-11	31.4
11 MHz	4.52e-8	5.04e-13	4.21e-11	0.17	2.47e-10	22.6

Table 4.5: SNR due to Shot+Thermal noise for 11 MHz bandwidth (reference model)

Frequency	Signal Variance (A^2)	Shot noise Variance (A^2)	Thermal Noise (V^2)	Gain (R^2)	Thermal Noise Variance (A^2)	SNR in dB
10 kHz	4.52e-8	1.1099e-13	4.74e-14	97.6	4.85e-16	56.1
100 kHz	4.52e-8	1.1099e-13	8.56e-13	121.9	7.02e-15	55.8
700 kHz	4.52e-8	1.1099e-13	7.46e-12	32.5	2.29e-13	51.2
1 MHz	4.52e-8	1.1099e-13	8.22e-12	18.2	4.51e-13	49.1
2 MHz	4.52e-8	1.1099e-13	8.95e-12	5.1	1.75e-12	43.9
4 MHz	4.52e-8	1.1099e-13	9.19e-12	1.3	7.06e-12	38
11 MHz	4.52e-8	1.1099e-13	9.26e-12	0.17	5.44e-11	29.2

4.2 Combined Noise Analysis

This section will find out the impact on SNR for both the models when the noises (Shot and Thermal) are combined together.

4.2.1 For Reference Model

Shot noise is calculated in terms of A^2 whereas Thermal noise in terms of V^2. To add both the noises, two methods can be used, either the shot noise can be converted in terms of V^2 by multiplying it with the receiver gain (which is in terms of R^2, or the thermal noise can be converted in terms of A^2 by dividing it with the receiver gain. In this work, the second method is chosen to add both the noises. The received information signal is 4.52x$10^{-8}A^2$.

As already discussed in Section 4.4.1, Shot noise variance will be same for all frequencies and will only change with system Bandwidth. Combined noise calculation for 50 MHz and 11 MHz bandwidth is shown in Table 4.4 and 4.5 respectively.

Table 4.6: SNR due to Shot+Thermal noise for 50 MHz bandwidth (designed model)

Frequency	Signal Variance (A^2)	Shot noise Variance (A^2)	Thermal Noise (V^2)	Gain (R^2)	Thermal Noise Variance (A^2)	SNR in dB
10 kHz	4.52e-8	5.04e-13	1.49e-14	10.98	1.35e-15	49.5
100 kHz	4.52e-8	5.04e-13	1.89e-13	14.6	1.29e-14	49.4
700 kHz	4.52e-8	5.04e-13	6.37e-12	11.08	5.74e-13	46.2
1 MHz	4.52e-8	5.04e-13	1.03e-11	8.8	1.17e-12	44.3
2 MHz	4.52e-8	5.04e-13	1.86e-11	3.97	4.68e-12	39.4
4 MHz	4.52e-8	5.04e-13	2.31e-11	1.23	1.87e-11	33.7
11 MHz	4.52e-8	5.04e-13	2.34e-11	0.16	1.46e-10	24.9

Table 4.7: SNR due to Shot+Thermal noise for 11 MHz bandwidth (designed model)

Frequency	Signal Variance (A^2)	Shot noise Variance (A^2)	Thermal Noise (V^2)	Gain (R^2)	Thermal Noise Variance (A^2)	SNR in dB
10 kHz	4.52e-8	1.1099e-13	3.29e-15	10.98	2.99e-16	56.1
100 kHz	4.52e-8	1.1099e-13	4.16e-14	14.6	2.84e-15	56
700 kHz	4.52e-8	1.1099e-13	1.4e-12	11.08	1.26e-13	52.8
1 MHz	4.52e-8	1.1099e-13	2.26e-12	8.8	2.56e-13	50.9
2 MHz	4.52e-8	1.1099e-13	4.09e-12	3.97	1.03e-12	46
4 MHz	4.52e-8	1.1099e-13	5.08e-12	1.23	4.13e-12	40.3
11 MHz	4.52e-8	1.1099e-13	5.15e-12	0.16	3.21e-11	31.5

4.2.2 For designed model

Combined noise calculation for 50 MHz, 11 MHz, 4 MHz and 2 MHz bandwidth is shown in Table 4.6, 4.7, 4.8 and 4.9 respectively.

Table 4.8: SNR due to Shot+Thermal noise for 4 MHz bandwidth (designed model)

Frequency	Signal Variance (A^2)	Shot noise Variance (A^2)	Thermal Noise Variance (A^2)	SNR in dB
10 kHz	4.52e-8	4.036e-14	1.08e-16	60.5
100 kHz	4.52e-8	4.036e-14	1.03e-15	60.4
700 kHz	4.52e-8	4.036e-14	4.59e-14	57.2
1 MHz	4.52e-8	4.036e-14	9.36e-14	55.3
2 MHz	4.52e-8	4.036e-14	3.72e-13	50.4
4 MHz	4.52e-8	4.036e-14	1.5e-12	44.7
11 MHz	4.52e-8	4.036e-14	1.16e-11	35.9

Table 4.9: SNR due to Shot+Thermal noise for 2 MHz bandwidth (designed model)

Frequency	Signal Variance (A^2)	Shot noise Variance (A^2)	Thermal Noise Variance (A^2)	SNR in dB
10 kHz	4.52e-8	2.018e-14	5.44e-17	63.5
100 kHz	4.52e-8	2.018e-14	5.18e-16	63.4
700 kHz	4.52e-8	2.018e-14	2.29e-14	60.2
1 MHz	4.52e-8	2.018e-14	4.68e-14	58.3
2 MHz	4.52e-8	2.018e-14	1.87e-13	53.4
4 MHz	4.52e-8	2.018e-14	7.52e-13	47.7
11 MHz	4.52e-8	2.018e-14	5.85e-12	38.9

Table 4.10: Comparison of SNR due to Shot noise only

Input Frequency	Reference model SNR (in dB)		New model SNR (in dB)			
	B=50 MHz	B=11 MHz	B=50 MHz	B=11 MHz	B=4 MHz	B=2 MHz
10 kHz	49.5	56.1	49.5	56.1	60.5	63.5
100 kHz	49.5	56.1	49.5	56.1	60.5	63.5
700 kHz	49.5	56.1	49.5	56.1	60.5	63.5
1 MHz	49.5	56.1	49.5	56.1	60.5	63.5
2 MHz	49.5	56.1	49.5	56.1	60.5	63.5
4 MHz	49.5	56.1	49.5	56.1	60.5	63.5
11 MHz	49.5	56.1	49.5	56.1	60.5	63.5

4.3 Results and conclusion

Noise contribution due to Shot noise and Thermal noise independently and in combination is studied and the results for both the models were shown in previous sections. The comparison chart of both the models is shown in this section in Table 4.10, 4.11 and 4.12.

As already discussed, Shot noise will not change with the change in frequency. So at any frequency value, SNR is same for both the circuits. However, with the decrease in system Bandwidth, SNR is improving.

As it is clear from the comparison tables for Thermal and Combined noises, that with the increase in frequency the Signal to Noise ratio will keep on decreasing and with the decrease in system Bandwidth the SNR is improving. The designed model is giving better SNR values than the reference model, at same Bandwidth and frequency.

Table 4.11: Comparison of SNR due to Thermal noise only

Input Frequency	Reference model SNR (in dB)		New model SNR (in dB)			
	B=50 MHz	B=11 MHz	B=50 MHz	B=11 MHz	B=4 MHz	B=2 MHz
10 kHz	73.1	79.6	75.2	81.7	86.1	89.1
100 kHz	61.5	68.1	65.4	72	76.3	79.4
700 kHz	46.3	52.9	48.9	55.5	59.9	62.9
1 MHz	43.4	50	45.8	52.4	56.8	59.8
2 MHz	37.5	44.1	39.8	46.4	50.8	53.8
4 MHz	31.5	38.1	33.8	40.4	44.7	47.8
11 MHz	22.6	29.2	25	31.6	36	39

Table 4.12: Comparison of SNR due to Combined noise (Shot+Thermal)

Input Frequency	Reference model SNR (in dB)		New model SNR (in dB)			
	B=50 MHz	B=11 MHz	B=50 MHz	B=11 MHz	B=4 MHz	B=2 MHz
10 kHz	49.5	56.1	49.5	56.1	60.5	63.5
100 kHz	49.3	55.8	49.4	56	60.4	63.4
700 kHz	44.7	51.2	46.2	52.8	57.2	60.2
1 MHz	42.5	49.1	44.3	50.9	55.3	58.3
2 MHz	37.3	43.9	39.4	46	50.4	53.4
4 MHz	31.4	38	33.7	40.3	44.7	47.7
11 MHz	22.6	29.2	24.9	31.5	35.9	38.9

Chapter 5

Conclusion and Future Work

5.1 Conclusion

Using a solar panel in the receiver circuit as a photo detector and by optimizing the load parameters, the communication results can be improved in terms of Bandwidth, output pulse shape and Signal to Noise ratio.

In chapter three, a new receiver model is presented which is a modification of the existing model presented in chapter two. It can be seen from the results that with the change in load parameters, the bandwidth of the system can be improved. The achieved bandwidth is 2 MHz. Also, the shape of the output pulse can be retained to a great extent with the use of an equalizer circuit. Even after giving the random pulse as an input to the system, the same pattern of output pulse is achievable upto certain extent.

In chapter four, noise analysis part is covered, which clearly shows a better SNR with the new designed model. SNR due to Shot noise is constant for both the models and due to Thermal noise it is higher for the designed model with the SNR of 52.4 dB at 1 MHz of input frequency and system bandwidth of 11 MHz. SNR due to combined Shot and Thermal noises is also calculated for both the models (reference and new design), which was not calculated in the reference paper, and the same is also turned out to be better in case of new model at different input frequencies and system bandwidths. For input frequency range of 700 kHz- 2 MHz and system bandwidth of 11 MHz, it is giving 52.8-46 dB of SNR value as compared to 51.2-43.9 dB of reference model.

5.2 Future work

- The design proposed in Chapter 3 can be used to improve the bandwidth of the system in a communication system and with further modifications a higher data rate can be achieved with this model. Output pulse shape can be further improvised by selecting a suitable equalizer circuit.
- Adding an additional equalizer circuit results in decrease of output signal amplitude. This can be compensated by adding an amplifier at the output of the receiver circuit.

Bibliography

[1] Z. Wang, D. Tsonev, S. Videv, and H. Haas, "On the design of a solar-panel receiver for optical wireless communications with simultaneous energy harvesting," *IEEE Journal on Selected Areas in Communications*, vol. 33, no. 8, pp. 1612–1623, 2015.

[2] H. Elgala, R. Mesleh, and H. Haas, "Indoor optical wireless communication: potential and state-of-the-art," *IEEE Communications Magazine*, vol. 49, no. 9, pp. 56–62, 2011.

[3] T. Komine and M. Nakagawa, "Fundamental analysis for visible-light communication system using led lights," *IEEE transactions on Consumer Electronics*, vol. 50, no. 1, pp. 100–107, 2004.

[4] G. Keiser, "Optical fiber communications," *Wiley encyclopedia of telecommunications*, 2003.

[5] Z. Wang, D. Tsonev, S. Videv, and H. Haas, "Towards self-powered solar panel receiver for optical wireless communication," in *2014 IEEE International Conference on Communications (ICC)*. IEEE, 2014, pp. 3348–3353.

[6] S. Zhang, D. Tsonev, S. Videv, S. Ghosh, G. A. Turnbull, I. D. Samuel, and H. Haas, "Organic solar cells as high-speed data detectors for visible light communication," *Optica*, vol. 2, no. 7, pp. 607–610, 2015.

[7] E. Lorenzo, *Solar electricity: engineering of photovoltaic systems.* Earthscan/James & James, 1994.

[8] G. Walker *et al.*, "Evaluating mppt converter topologies using a matlab pv model," *Journal of Electrical & Electronics Engineering*, vol. 21, no. 1, pp. 49–56, 2001.

[9] D. Sera, R. Teodorescu, and P. Rodriguez, "Pv panel model based on datasheet values," in *2007 IEEE international symposium on industrial electronics.* IEEE, 2007, pp. 2392–2396.

[10] F. Adamo, F. Attivissimo, A. Di Nisio, and M. Spadavecchia, "Characterization and testing of a tool for photovoltaic panel modeling," *IEEE Transactions on Instrumentation and Measurement*, vol. 60, no. 5, pp. 1613–1622, 2011.

[11] D. Rusirawan and I. Farkas, "Identification of model parameters of the photovoltaic solar cells," *Energy Procedia*, vol. 57, pp. 39–46, 2014.

[12] P. A. Haigh, Z. Ghassemlooy, H. Le Minh, S. Rajbhandari, F. Arca, S. F. Tedde, O. Hayden, and I. Papakonstantinou, "Exploiting equalization techniques for improving data rates in organic optoelectronic devices for visible light communications," *Journal of lightwave technology*, vol. 30, no. 19, pp. 3081–3088, 2012.

[13] H. Le Minh, D. O'Brien, G. Faulkner, L. Zeng, K. Lee, D. Jung, Y. Oh, and E. T. Won, "100-mb/s nrz visible light communications using a postequalized white led," *IEEE Photonics Technology Letters*, vol. 21, no. 15, pp. 1063–1065, 2009.

[14] J. M. Kahn and J. R. Barry, "Wireless infrared communications," *Proceedings of the IEEE*, vol. 85, no. 2, pp. 265–298, 1997.

[15] G. P. Agrawal, *Fiber-optic communication systems.* John Wiley & Sons, 2012, vol. 222.